LITHOS 494-495 (2025) 107941

Contents lists available at ScienceDirect

LITHOS

journal homepage: www.elsevier.com/locate/lithos

New integrations of U—Pb zircon data from Caledonian intrusions in the Southern Uplands of Scotland

Chloe A.R. Gemmell [a,b], Iain Neill [a,*], Mark Wildman [a], Careen MacRae [a,c], David Currie [d], Joshua F. Einsle [a]

[a] Geographical and Earth Sciences, University of Glasgow, Glasgow G12 8QQ, Scotland, UK
[b] School of Geosciences, University of Aberdeen, Aberdeen AB24 3FX, Scotland, UK
[c] School of GeoSciences, University of Edinburgh, Edinburgh EH9 3FE, Scotland, UK
[d] British Geological Survey, Keyworth NG12 5GG, England, UK

ARTICLE INFO

Keywords:
Antecryst
Geochronology
Geodynamics
Scotland
Zircon

ABSTRACT

The Laurentian margin in Britain and Ireland experienced the Caledonian-Acadian orogenies resulting from Palaeozoic closure of the Iapetus Ocean and accretion of Baltica and peri-Gondwanan terranes. However, the age and significance of magmatism remain contested, without a geologically consistent geodynamic reconstruction. We have interrogated the U—Pb zircon record of intrusive complexes within the Southern Uplands-Down-Longford accretionary complex, focused on the Southern Uplands in Scotland. New texturally constrained laser ablation data are presented from the Carsphairn, Black Stockarton Moor, Bengairn, and Cheviot complexes. In these locations, most zircons contain poorly zoned cores with $^{206}Pb/^{238}U$ ages no older than ~ 424 Ma, chemically comparable with younger magmatic overgrowths. Magmatic overgrowth ages confirm emplacement of Carsphairn at ~ 414–411 Ma, Black Stockarton Moor and Bengairn at ~ 410–408 Ma, and Cheviot at ~ 400 Ma. Across the accretionary complex, the onset of zircon growth from ~ 424 Ma appears to mark slab roll-back processes. Zircon cores may represent stalling and crystallisation of magmas in the deep crust, whilst emplacement into the shallow crust after ~ 415 Ma accompanies the onset of regional transtension. We do not feel there is sufficient evidence to directly attribute magmatism to slab breakoff, despite this process being popularly championed in Scottish and Irish geology. We discuss the latest geodynamic interpretations of magmatism during the Caledonian-Acadian events, including events to the south of the Iapetus suture, and argue that complete zircon histories have a role to play in reconstruction of ancient orogens.

1. Introduction

Collision magmatism is a natural continuation of continental arc magmatism, occurring between the onset of continental collision and the end of continental convergence (Pearce et al., 1990; Turner et al., 1992; Williams et al., 2004). Collision magmatism is a contributor to the composition of the continental crust (Annen et al., 2006; Couzinié et al., 2016; Gómez-Frutos et al., 2023; Neill et al., 2015) and to ore deposits (Richards, 2009). Sources of melt depend on the thickness, composition, and thermal state of the lithosphere. Significant crustal melting is possible where the crust has been substantially thickened, such as the Himalayas (England and Thompson, 1986), whereas regions such as Turkey, the Caucasus, and Iran are characterised by more extensive melting of lithospheric and even asthenospheric mantle (Keskin, 2003; Neill et al., 2015). It has become popular to associate such mantle-derived magmatism to processes such as lithospheric delamination (e.g., Pearce et al., 1990) and breakoff of the oceanic lithosphere (e.g., Keskin, 2003 and many others). There is also recognition of the importance of crustal stress in the location of magmatism, emplacement depths, and ore-forming potential (e.g., Chiaradia, 2022; Miles et al., 2016). However, in ancient orogenic belts, the role of geodynamic processes in collision magmatism can be equivocal.

The Southern Uplands of Scotland and the Down-Longford Terrane in Ireland are part of the Palaeozoic Caledonian-Acadian Belt. This location is a natural laboratory to investigate the occurrence of magmatism during and immediately following continental collision (Fig. 1). These terranes represent a former accretionary prism above a north-dipping Iapetus subduction zone (Leggett, 1987; Leggett et al., 1982). A

* Corresponding author.
E-mail address: iain.neill@glasgow.ac.uk (I. Neill).

https://doi.org/10.1016/j.lithos.2024.107941
Received 31 May 2024; Received in revised form 23 December 2024; Accepted 27 December 2024
Available online 6 January 2025
0024-4937/© 2025 The Authors. Published by Elsevier B.V. This is an open access article under the CC BY license (http://creativecommons.org/licenses/by/4.0/).

window of plutonic and volcanic emplacement from ~415–385 Ma postdates the onset of collision between peri-Gondwanan terranes and Laurentia (Brown et al., 2008). Magmatism has been of interest owing to minor occurrences of mineralisation (e.g., Brown et al., 1979a; Leake et al., 1977; Rice et al., 2018). There are detailed local geochronological and geochemical studies (e.g., Cooper et al., 2016; Fritschle, 2016; Hines et al., 2018; Miles et al., 2014; and references therein), and a body of work on magmatism further north in the Grampian Highlands of Scotland (e.g., Miles et al., 2016; Neilson et al., 2009; Oliver et al., 2008; and references therein). Yet, as this study describes, the igneous record has been interpreted in different ways regarding the geometries of Iapetus subduction and continental collision. A further layer of complexity comes from the presence of voluminous magmatism of a similar age south of the Iapetus suture (Selby et al., 2008), highlighting the need for a geologically robust geodynamic model. We therefore aim to 1) provide new U—Pb geochronological data for three plutons and a sub-volcanic complex in the Southern Uplands of Scotland, 2) integrate these data with published work from across the Southern Uplands-Down-Longford terranes, 3) propose a geologically consistent geodynamic model which explains the patterns of magmatism for this sector of the Laurentian margin, and 4) contribute to discussion on the origin of contemporaneous magmatism south of the Iapetus suture in Ireland and Northern England. The work also has the broader objective of highlighting the importance of the trans-crustal nature of magmatism in geochronological studies, and that an overt focus on relating emplacement ages to deep geodynamics is inherently problematic (e.g., Milne et al., 2023).

2. Geological background

2.1. The Iapetus Ocean and the Laurentian accretionary prism

The Cambrian to Devonian closure of the Iapetus Ocean and associated tectonism between Laurentia, Baltica, and peri-Gondwanan terranes define the Caledonian and Acadian Orogenies in Britain and Ireland (Archibald and Murphy, 2021; Chew and Strachan, 2014; Lambert and McKerrow, 1976; McKerrow et al., 2000; Oliver et al., 2008). North of the Iapetus Suture, Scotland and Ireland are divided into terranes belonging to the Laurentian margin, each experiencing one or more compressional tectonic episodes (Fig. 1). The Northern and Grampian Highland terranes record the Grampian Orogeny (c. 475–460 Ma), representing collision of the Midland Valley terrane with the Laurentian margin (Bird et al., 2013). A subsequent Grampian II event (~450 Ma) is recorded in the Northern Highlands terrane and is of debated origin (Bird et al., 2013; Dewey et al., 2015; Milne et al., 2023).

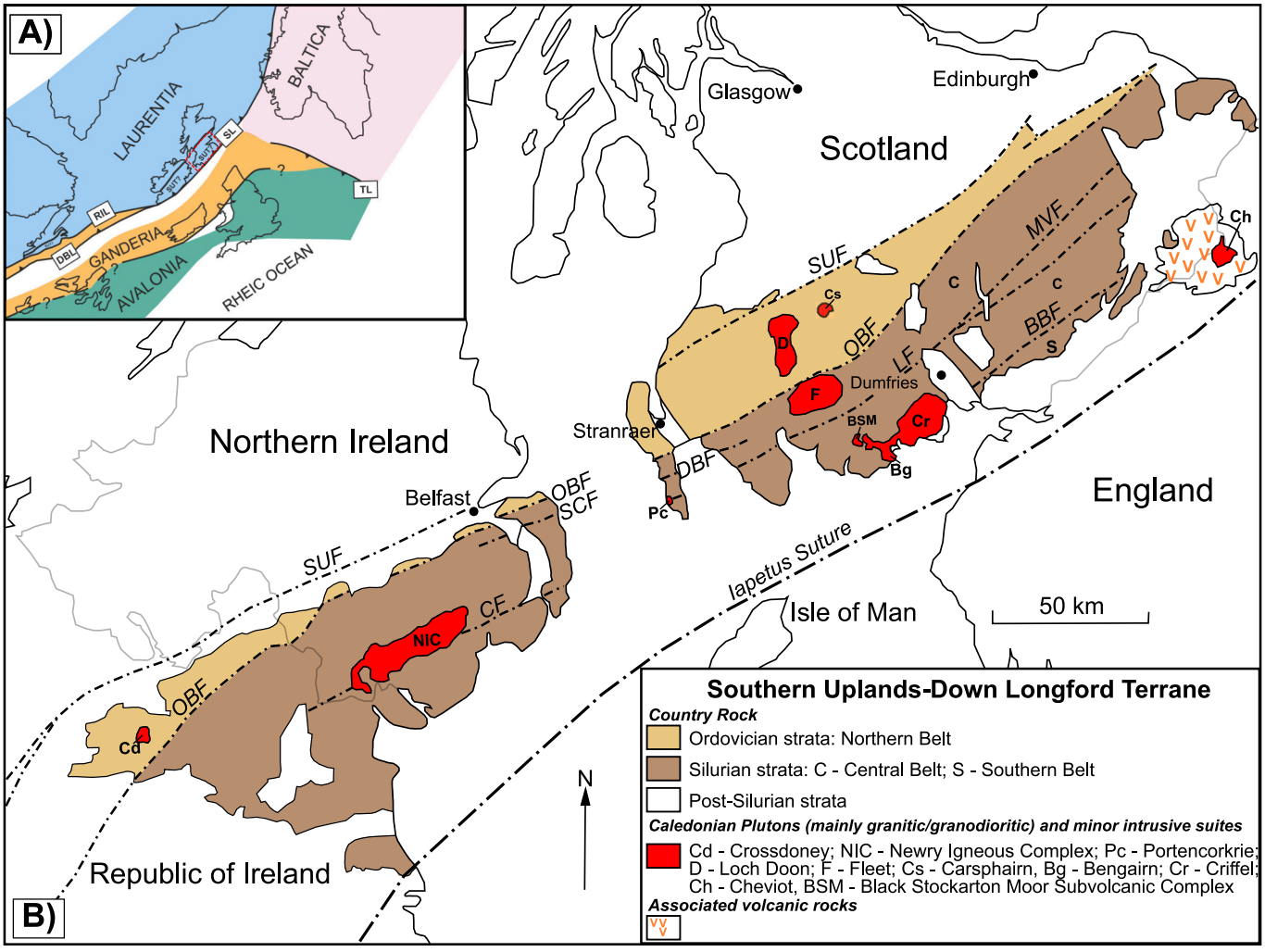

Fig. 1. a) Palaeogeographical plate reconstruction at ~420 Ma (not to scale). DBL = Dog Bay Line; RIL = Red Indian Line; SL = Solway Line; TL = Tornquist Line. Adapted from Waldron et al. (2014). b) Locations of Caledonian plutons, intrusive suites, volcanism, and major faults across the Southern Uplands-Down-Longford Terrane. OBF = Orlock Bridge Fault; CF = Cloghy Fault; SUF = Southern Uplands Fault; SCF = Southern Coalpit Bay Fault; DBF = Fault; LF = Laurieston Fault; BBF = Balmae Burn Fault; MVF = Moffat Valley Fault. Adapted from Stone et al. (2012), Miles et al. (2014) and Cooper et al. (2016). (For interpretation of the references to colour in this figure legend, the reader is referred to the web version of this article.)

The Scandian Orogeny (~435–417 Ma) in the Northern Highlands terrane records oblique terminal collision between Baltica and Laurentia and the end of Iapetus subduction beneath this terrane (Strachan et al., 2020).

At the onset of the Scandian Orogeny, the Grampian Highlands, Midland Valley, and Southern Uplands-Down-Longford terranes were located southwest of the Northern Highlands and continued to lie above the Iapetus slab (Dewey and Strachan, 2003). The Southern Uplands-Down-Longford Terranes are now widely considered to represent the accretionary forearc (Leggett, 1987; Leggett et al., 1982; Stone, 2024), with the active continental arc sited further north, where an extensive magmatic record is preserved (Oliver et al., 2008; Thirlwall, 1988). The accretionary complex started growing after obduction of the Ballantrae ophiolite and initiation of northward subduction of Iapetus oceanic lithosphere (Chew and Strachan, 2014). The complex consists of tracts of submarine pelagic sediments, continent-derived siliciclastic material, and volcaniclastic rocks (Stone et al., 2012). North-verging thrust sheets generated successively younger northern, central, and southern belts with their own internal stratigraphy (Leggett et al., 1982). The duration of accretion was from ~455 – ~420 Ma (Brown et al., 2008; Chew and Strachan, 2014; Leggett et al., 1982; Oliver et al., 2008). Late in the accretion process, docking of various terranes began, starting with the Leinster-Lakesman terrane (Fig. 1, e.g., Waldron et al., 2014 and references therein), followed by Avalonia, triggering the Acadian Orogeny from ~404–394 Ma in Northern England (Woodcock et al., 2007; Woodcock et al., 2019).

2.2. Collision magmatism and geochronology

Magmatic emplacement in the accretionary complex only occurred after termination of sedimentation into the accretionary prism, with typical emplacement ages based on a variety of Rb—Sr and U—Pb methods ranging from ~415–385 Ma (see Table 1). Magmatism of similar age and older is also found in the Midland Valley and the Grampian Highlands (Badenszki et al., 2019; Neilson et al., 2009; Oliver et al., 2008; Thirlwall, 1982; Thirlwall, 1988). Magmatism is therefore

Table 1
Summary of igneous bodies associated with collision magmatism in the Southern Uplands of Scotland and the Down-Longford Terrane of Northern Ireland and the Republic of Ireland. Bodies are presented in approximate order of reported emplacement age, though some have a range of emplacement ages for different facies. Rb—Sr data are reported to 2σ, recalculated with the revised ^{87}Rb decay constant of Villa et al. (2015). U—Pb zircon data are reported as weighted mean ^{206}Pb/^{238}U ages to 2σ as published, except for the Crossdoney pluton, Ireland, where results were re-calculated having originally been published as a weighted mean ^{207}Pb/^{206}Pb age. Abbreviations: CBS = Central Belt of the Southern Uplands in Scotland; SBS = Southern Belt of the Southern Uplands in Scotland. NBS = Northern Belt of the Southern Uplands in Scotland. I = Ireland. E = England. WR = whole rock. Ap = apatite. Bt = biotite. Ms. = muscovite. Px = pyroxene. Amp = amphibole. F = feldspar. IMP = ion microprobe. LA-ICP-MS = laser ablation inductively coupled plasma mass spectrometry. TIMS = isotope dilution thermal ionisation MS.

Name	Location and type of magmatism	Rb-Sr age (N) or *Re*—Os (S)	Method	U-Pb zircon-derived time of emplacement	Ages of antecrystic zircon growth	Method	References
North of the Iapetus Suture							
Fleet	CBS pluton	399.4 ± 2.1	Bt-Ms WR	387 ± 5 Ma for inner muscovite granite; 410 ± 3 Ma for outer biotite granite	Not identified	U-Pb IMP	Halliday et al., 1980; Miles et al., 2014
Portencorkrie	CBS pluton	399.9 ± 19.4	WR	395 ± 9 Ma	Not identified	U-Pb IMP	Evans (1995); Oliver et al., 2008
Doon	NBS pluton	416.5 ± 1.5	Bt-WR	396.7 ± 4.3 Ma for outer quartz diorite; other zones provided older ages interpreted as antecrystic or inherited	~416–424 Ma	U-Pb LA-ICP-MS	Halliday et al., 1980; Hines et al., 2018
Cheviot	SBE + S pluton and volcanic complex	403.8 ± 3.0 403.8 ± 3.9	Bt-WR Bt-Ap	400.0 ± 2.9 Ma for granophyre facies in plutonic complex; 400.1 ± 4.7 Ma for Standrop facies in plutonic complex	Up to ~417 Ma	U-Pb LA-ICP-MS	Thirlwall, 1988; this study
Black Stockarton Moor and Bengairn	CBS sub-volcanic minor intrusions; CBS pluton	Not analysed	n/a	Range from 407.8 ± 2.9 to 410.2 ± 1.7 Ma where an age could be confidently defined	Up to ~424 Ma	U-Pb LA-ICP-MS	This study
Criffell-Dalbeattie	CBS pluton	404.2 ± 2.0	Bt-WR	Range from 408 ± 14 to 412 ± 5 Ma for four zones out of five identified. Overall emplacement age of 410 ± 6 Ma	Not identified	U-Pb IMP	Halliday et al., 1980; Miles et al., 2014
Newry	CBI plutonic complex	Range from 411.1 ± 3.1 to 407 ± 3.1	WR	Range from 414.0 ± 0.2 to 410.3 ± 0.2 Ma for three zones (Seeconnell, Rathfriland, Newry) and 407.2 ± 0.4 Ma for a younger zone (Cloghoge)	~415 Ma, in Rathfriland zone	U-Pb TIMS	O'Connor, 1975; Cooper et al., 2016
Cairnsmore of Carsphairn	NBS pluton	418.6 ± 4.1	WR	Range from 410.5 ± 1.8 to 412.7 ± 4.7 Ma where an age could be confidently defined	Up to ~424 Ma	U-Pb LA-ICP-MS	Thirlwall, 1988; this study
Crossdoney	NBI pluton	Not analysed	n/a	Granite re-interpreted as 413.2 ± 1.7 Ma (n = 18, MSWD = 0.8)	Not argued for in original study but likely up to ~425 Ma as re-interpreted.	U-Pb IMP	Fritschle, 2016), re-interpreted here
South of the Iapetus Suture							
Shap	Lakesman pluton	405.2 ± 1.8	Re-Os	Miles and Woodcock (2018)) did not provide an emplacement age but reverted to existing Re—Os and Rb—Sr data	Up to ~428 Ma	U-Pb IMP	Selby et al., 2008; Miles and Woodcock, 2018
Skiddaw	Lakesman pluton	398.8 ± 0.4 392.3 ± 0.8	Re-Os	Not available	Not identified	n/a	Selby et al., 2008
Weardale	Lakesman batholith	398.3 ± 1.6	Re-Os	Concordia 399.34 ± 0.68 (*n* = 2); re-interpreted 397.5 ± 0.4 Ma (*n* = 4, MSWD = 0.41)	Not identified	U-Pb TIMS	Selby et al., 2008; Kimbell et al., 2010
Leinster	Leinster batholith	Not analysed	n/a	Range from 404.9 ± 2.6 to 417.4 ± 1.7 Ma	Not identified	U-Pb LA-ICP-MS	Fritschle et al., 2018

inherently 'collisional' in nature, comparable with modern settings such as Eastern Anatolia and the Caucasus (Keskin, 2003; Pearce et al., 1990). Many plutonic bodies in the accretionary complex have concentric facies zonation, attributed to fractional crystallisation and hybridisation processes as well as the emplacement of compositionally distinct magma types (e.g., Thirlwall, 1988; Anderson et al., 2016; Tindle et al., 1988). Zircon U—Pb dates and Hf—O isotopes have been used to identify three primary sources of melt: the upper mantle, underthrust peri-Gondwanan lithosphere, and the accretionary complex itself (e.g., Miles et al., 2014). Zircons in individual plutons have recently been found to include populations of antecrysts which grew prior to emplacement (Cooper et al., 2016; Hines et al., 2018; Miles et al., 2014). In the case of the Doon pluton (Table 1), some facies have zircon ages significantly older than field relationships permit, implying earlier formed crystal mushes were remobilised and later crystallised during emplacement without generating datable new zircon growth (Hines et al., 2018). To explore geodynamic processes further, a fuller picture of both the timing of emplacement and especially the longevity of magmatic systems in this region is necessary. Despite much available geochronology, some intrusive complexes have only been dated by whole-rock or mineral Rb—Sr methods (e.g., Thirlwall, 1988), which, though providing valuable and accurate data about emplacement geochronology, cannot constrain pre-emplacement processes (Table 1; Law et al., 2024). A similar evolution of dating approaches has taken place on contemporaneous magmatism immediately to the south of the Iapetus suture, also including Re—Os methods on sulfides. Magmatism in this region includes the Leinster Batholith in Ireland (e.g., Fritschle et al., 2018) and the Shap, Skiddaw and Weardale granites in England (Selby et al., 2008; Kimbell et al., 2010; Miles and Woodcock, 2018). Their geodynamic significance is explored in the Discussion, below.

2.3. Magmatic complexes in this study

This study focuses on several intrusive complexes which presently lack U—Pb zircon geochronology, including the Carsphairn pluton, the Black Stockarton Moor sub-volcanic complex and Bengairn pluton, and the Cheviot volcano-plutonic complex, all in the Southern Uplands of Scotland. The following descriptions include revised Rb—Sr dates following adjustment of the ^{87}Rb decay constant (Villa et al., 2015).

2.3.1. Carsphairn

The Carsphairn Pluton (11 km^2) is ~7 km northeast of the Doon Pluton in the northern belt of the Southern Uplands (Fig. 2). It has a previously published Rb—Sr whole rock age of 418.6 ± 4.1 Ma (n = 2) from Thirlwall (1988). The pluton is compositionally zoned from an outer less evolved quartz diorite to a more evolved granitic centre. Previous studies based on whole rock and mineral geochemistry identified fractional crystallisation and hybridisation as important processes in petrogenesis, with Tindle et al. (1988) proposing quartz diorite and granodiorite facies to be genetically related, and the inner fine and coarse granites to be a slightly younger phase of intrusion related to mobilisation of a deeper-stored body of magma.

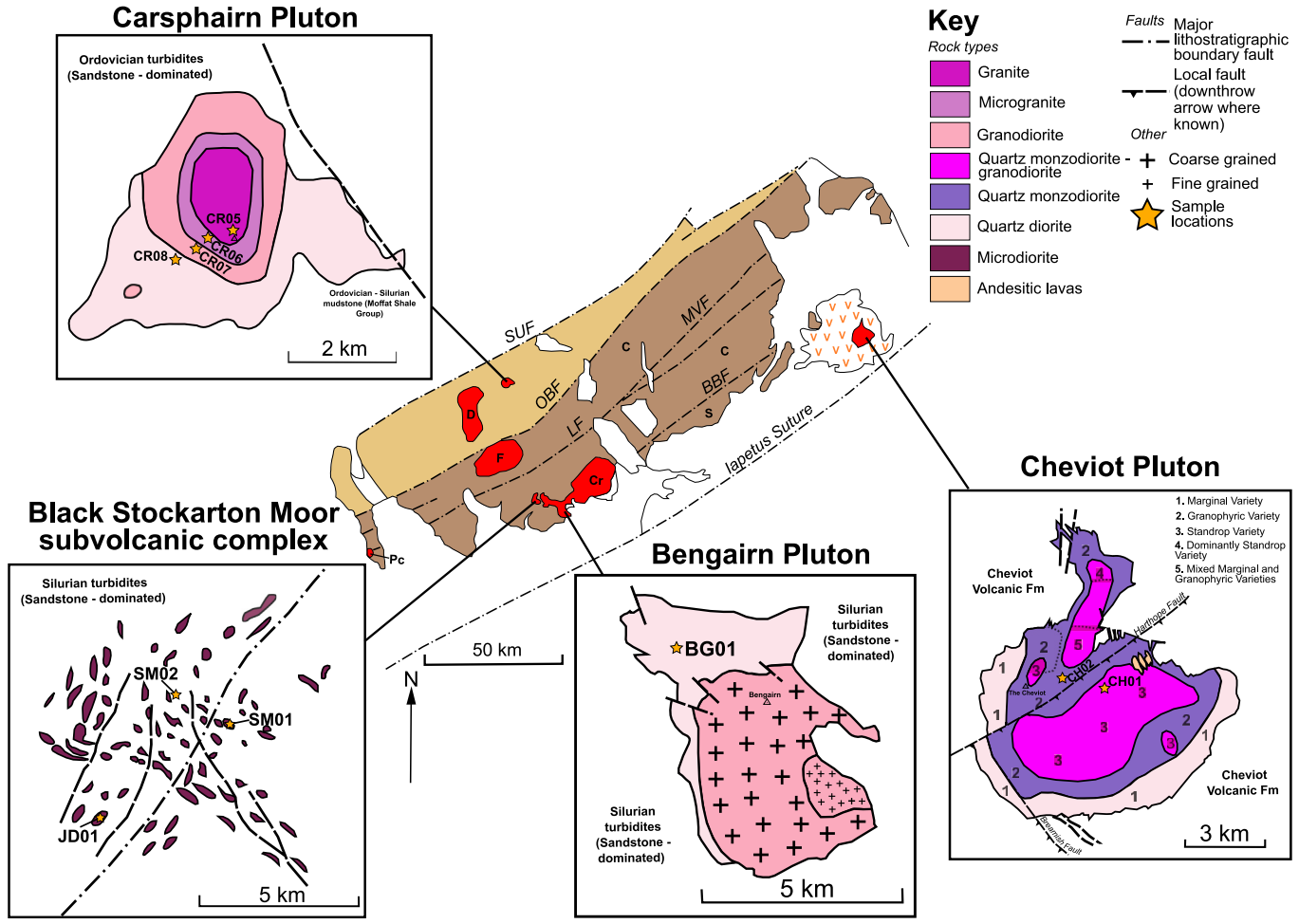

Fig. 2. Geological map of the Southern Uplands Terrane showing the Northern and Southern belts. Insets show key lithologies, faults and approximate sample locations for the studied magmatic complexes. See Fig. 1 for Southern Uplands-Down-Longford Terrane map key. Adapted from Hines et al. (2018); Stone et al. (2012); Jhingran (1942) and Al-Hafdh (1985).

2.3.2. Black Stockarton Moor and Bengairn

The Black Stockarton Moor sub-volcanic complex extends over >100 km^2, with minor intrusions predominantly striking NW-SE and NE-SW. A further ~15 km^2 area extensively cut by minor intrusions lies SE of the Bengairn and Criffell-Dalbeattie complexes (Fig. 2). Black Stockarton Moor comprises mafic to intermediate porphyritic dykes, sheets, stocks, and breccia "pipes" categorised by cross-cutting relationships and petrography into three generations (Brown et al., 1979a; Leake and Cooper, 1983); Table 2). The Bengairn pluton is cut by the third and youngest phase of minor intrusions at Black Stockarton Moor, whilst the Criffell-Dalbeattie pluton post-dates the entire complex (Brown et al., 1979a; Halliday et al., 1980; Leake and Cooper, 1983; Miles et al., 2014). The presence of mineralisation supports shallow crustal emplacement of the complex, recognised as a post-collisional porphyry Cu system during the British Geological Survey Mineral Reconnaissance Programme (Brown et al., 1979a; Leake and Cooper, 1983). Miles et al. (2014) instead treated Bengairn and Criffell-Dalbeattie as a single body, with Bengairn included in the outermost (oldest) part of the complex. Bengairn is compositionally zoned from a quartz diorite marginal zone to a granodiorite core.

2.3.3. Cheviot volcano-plutonic complex

Cheviot consists of a circular exposure of >700 km^2, comprising intermediate to felsic volcanic rocks surrounding ~70 km^2 of exposed plutonic rocks. The plutonic rocks are proposed to be intruding their own volcanic carapace (Al-Hafdh, 1985; Thirlwall, 1979). Mapping, geophysics, petrography, and geochemistry have been used to debate the origins and emplacement of the plutonic rocks. The plutonic complex ranges from marginal quartz diorite to a quartz monzodiorite-granodiorite core (Al-Hafdh, 1985; Jhingran, 1942). Our sampling comes from separate Standrop and granophyre facies according to the original mapping of Jhingran (Jhingran, 1942), which Al-Hafdh (Al-Hafdh, 1985) considered to belong to a unified Standrop facies (Table 2). Thirlwall (1988) provided three Rb—Sr dates of 399 ± 8 Ma (whole rock – plagioclase; n = 2), 388 ± 11 (whole rock – clinopyroxene; n = 2), and 404 ± 4 Ma (biotite, n = 2), for the volcanic rocks. For the plutonic rocks, a combination of whole rock, biotite, feldspar, and pyroxene Rb—Sr dates ranged from 402.1 ± 5.5 to 406.4 ± 5.2 Ma.

3. Methodology

New samples for geochronology were taken from the complexes listed in Table 2 during fieldwork in 2022 and 2023 and were prepared and analysed at the University of Glasgow. Rock samples were inspected by thin section for the presence of accessory phases. Selected samples were passed through a Retsch jaw crusher and sieved to obtain 90–500 μm size fractions. Standard shaking table, heavy liquid and electromagnetic separation methods were then used to isolate zircon crystals for mounting on resin pucks. Secondary electron and cathodoluminescence imaging were carried out using a Quanta 200F environmental scanning electron microscope at the Geoanalytical Electron Microscopy and Spectroscopy (GEMS) facility at the University of Glasgow. A sub-set of zircons from each sample were selected for laser ablation - inductively coupled plasma mass spectrometry (LA-ICP-MS) analysis. Site selection on each grain was based on the availability of zones of >30 μm width, devoid of visible alteration, fracturing, and mineral inclusions. Where possible, two sites were selected within each zone, the first for U—Pb geochronology and the second reserved for trace element analysis. The number of points analysed was limited by the total budget, and preference was given to obtaining U—Pb data over trace element analysis.

For U—Pb geochronology, LA-ICP-MS analysis was conducted on all samples using an Australian Scientific Instruments RESOlution laser with 3.3 J fluence and 10 Hz repetition rate. Spot size was 30 μm and ablation lasted 30 s per spot. Material was carried in Ar to a Thermo iCAP-RQ single collector mass spectrometer in the Themochronology

Table 2
Summary of the studied igneous complexes, with sample names and grid references marked in **bold**. The phase or facies names and their descriptions are adapted from the numbered references as follows: [1]Jhingran (1942); [2]Al-Hafdh (1985); [3]Stone et al. (2012); [4]Brown et al. (1979a); [5]Leake and Cooper (1983); [6]MacGregor (1937); [7]Tindle et al. (1988).

Phases	Descriptions and samples	Comments
Cheviot plutonic complex		
Granophyre[1]	Pink, coarse alkali feldspar granite **(CH-02, NT 9232 2047)**	[2]replaced the granophyre with a smaller Hedgehope granodiorite facies. In this interpretation, CH-01 and CH-02 would both belong to the Standrop facies, despite petrographic differences between the two.
Standrop[1]	Pale grey, coarse granodiorite **(CH-01, NT 9369 2041)**	[2]includes a smaller Dunhope granodiorite in the south of the complex prior to intrusion of the Standrop facies.
Marginal[1]	Fine quartz diorite[1]	Intrudes its own volcanic carapace comprising the Cheviot lavas and associated rocks.
Bengairn pluton		
Granodiorite[3, 6]	Fine to medium grained granodiorite[6].	Intruded into the quartz diorite. Heterogeneous throughout. Has been divided into 3 groups based on field, petrographic and chemical characteristics (e.g., G1, G2 and G3 of MacGregor (1937)).
Quartz diorite[3, 6]	Fine to medium plagioclase-dominated quartz monzodiorite **(BG-01, NX 772538)**	Emplaced first, prior to successive emplacement of granodiorite [6]. Bengairn pluton crosscuts Black Stockarton Moor Phase 1 dykes and is crosscut by Black Stockarton Moor Phase 2 dykes [5].
Black Stockarton Moor sub-volcanic complex		
Phase 3[4, 5]	*E*-W-trending microgranodiorite dykes[4]	Located S of the complex near Jordieland, are closely related to E-W faulting and cut Phase 1 and Phase 2 dykes [5].
Phase 2[4,5]	NW-SE trending mafic to intermediate dykes[4]	
	NW-SE-trending fine to medium plagioclase-dominated quartz diorite dykes (**SM-01, NX 73293 54,509)**	Associated with the Criffel-Dalbeattie pluton. Located around Sheilla Hill and Eldrick Hills and cut Phase 1 dykes[4,5]
Phase 1[4,5]	Plagioclase-dominated fine to medium quartz diorite sheets **(SM-02, NX 72427 54,975)**	Located around Black Stockarton Moor through to High Arkland. Sheets likely replace Phase 1 quartz diorite dykes and are cut by Phase 2 dykes [4,5]
	NE-SW-trending mafic dykes[4]	
	NE-SW-trending medium plagioclase-dominated quartz diorite dykes (**JD-01, NX 70947 53,015**)	Located to the N of Lochdougan Moor and around Jordieland [5].
Carsphairn pluton		
Granite[3]	Fine to medium alkali feldspar granite **(CR-05, NX 59450 98,020).**	Final phase of emplacement. Coarse grained due to lack of volatile loss and/or slow cooling [7].

(*continued on next page*)

Table 2 (*continued*)

Phases	Descriptions and samples	Comments
Microgranite[3]	Fine to medium plagioclase and quartz dominated granodiorite **(CR-06, NX 59088 97,913)**	Includes xenoliths and autoliths of quartz diorite. First pulse of granitic magmatism. Fine grained due to magma chilling and/or volatile loss [7].
Granodiorite[3]	Fine to medium plagioclase feldspar granodiorite **(CR-07, NX 58862 97,768)**	Xenoliths and autoliths (quartz diorite) imply granodiorite was emplaced after quartz diorite. Contain microgranite veins suggesting emplacement before microgranite [7].
Quartz diorite[3]	Fine to medium plagioclase feldspar monzogranite **(CR-08, NX 58562 97,559).**	Initial phase[7].

facility. Semi-random sample bracketing was used to scatter reference materials throughout each run, with an average of ~4 unknowns between reference materials. The data were generated in 4 separate runs and the raw data were processed in Iolite v.4 (Paton et al., 2011). Data were individually picked over to monitor ^{204}Pb counts. Where ^{204}Pb was above background levels, spots plotted to the right of the concordia on a Wetherill ^{206}Pb/^{238}U vs ^{207}Pb/^{235}U diagram, indicating a common Pb problem. These spots were therefore rejected from further interpretation. Data were also picked to remove components of signals associated with inclusions or Pb loss, and to snip signals where multiple zones were abraded. For each run, data were normalised to reference zircon 91,500 (^{206}Pb/^{238}U age of 1062.4 Ma ± 0.4 Ma, (Wiedenbeck et al., 1995), with Plešovice (^{206}Pb/^{238}U age of 337.1 ± 0.4 Ma, Sláma et al., 2008), Temora2 and NIST-610 as secondary standards. All individual and weighted mean ages are herein reported to 2σ (absolute). The Plešovice reference material produced weighted means of 340.1 ± 1.1 (MSWD = 0.8, $n = 18$) during analysis of SM02, 338.9 ± 1.2 Ma (MSWD = 1.2, $n = 21$) during analysis of CH01 and CR05, 340.1 ± 1.8 Ma (MSWD = 1, $n = 24$) during analysis of CH02, JD01 and CR06; and 336.7 ± 1.3 Ma (MSWD = 0.7, $n = 17$) during analysis of CR07 and CR08. No further correction was applied to individual spots, though the weighted mean ^{206}Pb/^{238}U ages are reported with the Stacey-Kramers common Pb correction, which had a minimal effect relative to the analytical point errors on each spot age (Stacey and Kramers, 1975).

Trace element analysis was conducted using the same laser ablation instrument to generate data from selected spots from samples CH01 (Cheviot) and CR07 and CR08 (Cairnsmore) in a single run. Each spot was selected immediately adjacent to spots which previously generated dates interpreted as representing antecrystic or emplacement-related growth. ^{91}Zr was used as an internal standard assuming 66 wt% ZrO_2, and results calibrated to reference zircon 91,500 and NIST-610. First relative standard deviations for the middle to heavy rare earth elements (REE) were around 1–10 %, 10–40 % for the lowest abundance light REE. Ti-in-zircon temperature was calculated with the formula of Watson et al. (2006).

4. Results

Rock sample descriptions are presented in the Supplementary Item A with this manuscript. Marked-up zircon cathodoluminescence images (Supplementary Item B), grain-by-grain descriptions (Supplementary Item C), and full geochronological (Supplementary Item D) and trace element (Supplementary Item E) data are presented in an enduring online repository at the University of Glasgow at: https://doi.org/10.5525/gla.researchdata.1780.

4.1. Cairnsmore of Carsphairn

4.1.1. Sample CR-08, NX 58562 97559

CR-08 is a monzogranite of 0.1–3 mm grain size. Plagioclase dominates with minor biotite, alkali feldspar, quartz and clinopyroxene and accessory apatite and zircon. Plagioclase and biotite are replaced with sericite, chlorite, epidote, and clay. From 105 imaged grains of CR-08, 55 grains were suitable for laser ablation, the high rejection rate being due to extensive fracturing. Selected grains were subhedral, typically ~100–275 μm in length, with larger cores than rims. Almost all grains have localised loss of zonation or bright patches related to fractures. The cores in CR-08 are typically complex with evidence of resorption and contain mostly faint and patchy oscillatory zoning. Overgrowths also have faint and patchy oscillatory zoning. As with the other samples from Carsphairn, some of the overgrowths have a narrow un-zoned dark rim, and in places there is little or no overgrowth, just a core with a narrow dark rim. From the 55 grains, 74 points were lasered and 53 of these there rejected due to observed discordance, Pb loss, and incorrect core-overgrowth age relationships. Of 21 points which all came from cores, there was a spread of ^{206}Pb/^{238}U ages from ~421–407 Ma (Fig. 3). No overgrowths produced acceptable concordant U—Pb data. Taken together, the 21 core points define an over-dispersed weighted mean ^{206}Pb/^{238}U age of 413.8 ± 1.2 Ma (MSWD = 2.6) (Fig. 3; Spencer et al., 2016). A single point which could not be texturally distinguished in terms of whether it came from a core or overgrowth had a ^{206}Pb/^{238}U age of ~427 Ma and is likely xenocrystic (Fig. 3).

4.1.2. Sample CR-07, NX 58862 97768

The sample is a granodiorite of 0.1–3 mm grain size with plagioclase and subordinate biotite, quartz and alkali feldspar and accessory zircon and titanite. Plagioclase and biotite are partially replaced with sericite, epidote, chlorite, and clay. Of 102 grains imaged, 70 were suitable for laser analysis, being mostly subhedral and ~ 110–375 μm in length, some up to ~675 μm. Most grains have moderate fracturing and associated alteration. Many of the grains have complex cores exhibiting some evidence of resorption and only faint and patchy oscillatory zoning. Overgrowths have very faint oscillatory zoning and occasional sector zoning. A dark un-zoned outer rim of variable width is present in most grains. 100 points across the 70 grains were lasered, with 62 of these rejected due to observed discordance, Pb loss, and incorrect core-overgrowth age relationships. The remaining 38 points came from overgrowths ($n = 8$) and cores ($n = 29$). The overgrowths ranged in age from ~424–412 Ma, producing a weighted mean ^{206}Pb/^{238}U age of 415.3 ± 1.7 Ma (MSWD = 1.7), the MSWD indicating slight over-dispersion (Fig. 3). Despite field evidence implying that there is a close spatial and temporal relationship between the four samples from Carsphairn, this age is outwith the confidence limit of sample CR-05 (see Section 5.1 for discussion). Of the cores, 12 points were within the confidence interval of the overgrowths, with a further 17 cores plotting between ~424–417 Ma, and a final 10 plotting between ~455–425 Ma (Fig. 3). Whilst some of the cores may be antecrystic and post-date the termination of sedimentation in the Southern Uplands accretionary prism, the oldest are more assuredly xenocrystic in nature.

4.1.3. Sample CR-06, NX 59088 97913

This rock is a granodiorite of 0.2–2.5 mm grain size. Plagioclase and quartz dominate with lesser alkali feldspar and biotite, and alteration of feldspar and biotite to sericite and clay. Accessories include zircon ± apatite. Of 110 grains mounted for CR-06, 66 were imaged and 42 deemed suitable for laser ablation. Complex internal textures are observed in most grains, which typically range from ~100–350 μm and up to ~800 μm. Most grains are subhedral with large cores and small rims, and modest amounts of fracturing and associated alteration. Cores are typically angular, with partial resorption in some. Around half the cores are un-zoned, otherwise zoning is faint and of sector or oscillatory type. Overgrowths have typically faint and patchy oscillatory zoning,

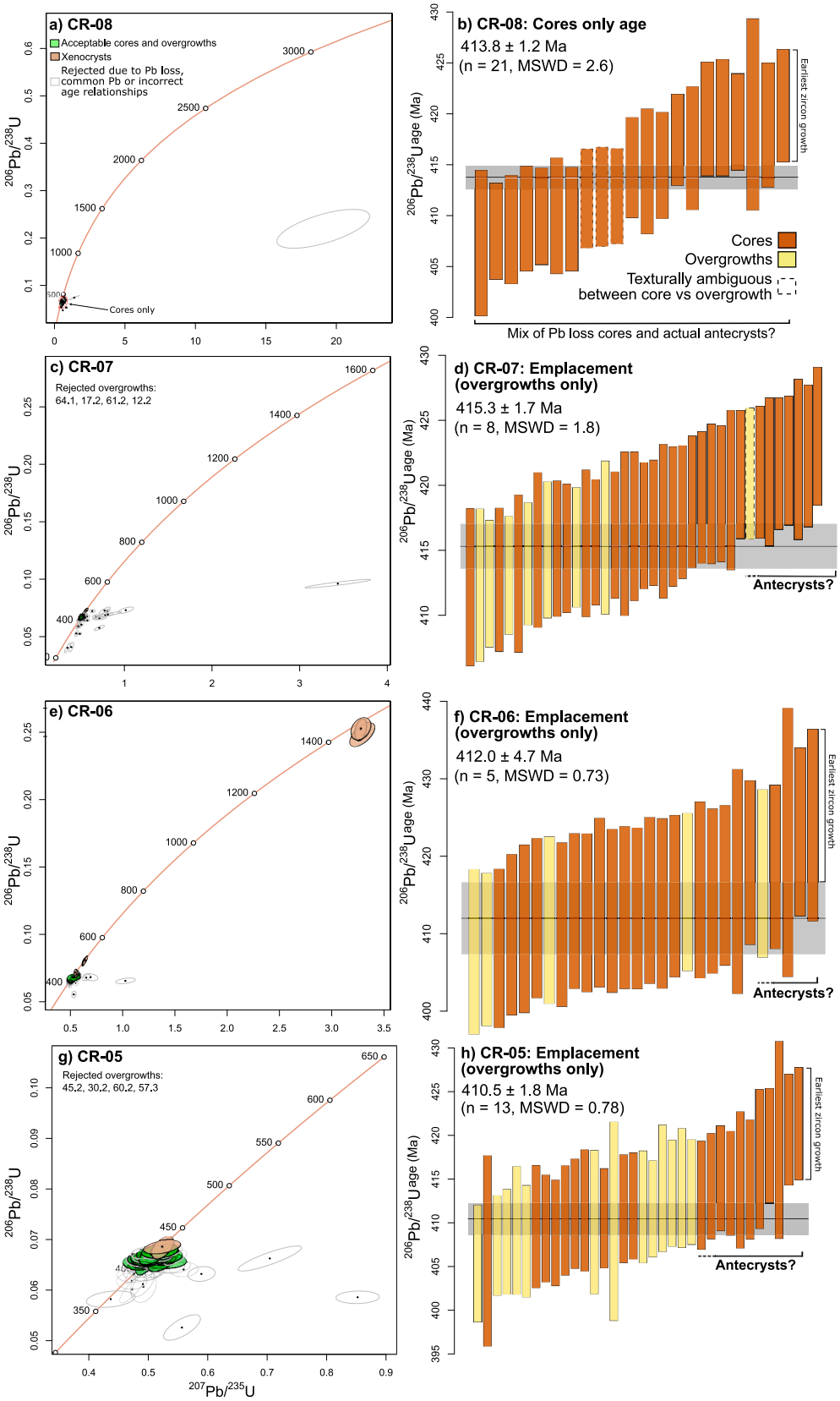

Fig. 3. Summary geochronological data for the Carsphairn Pluton including Wetherill Concordia plots before application of the Stacey Kramers common Pb correction and $^{206}Pb/^{238}U$ weighted mean plots shown after application of the common Pb correction. Samples presented include CR-08 (a – b), CR-07 (c – d), CR-06 (e – f) and CR-05 (g – h). The key for each sample is as per CR-08 unless otherwise stated.

with occasional sector zoning. As with CR-05, below, an outermost dark rim of variable width is present in most grains, in some cases representing the only growth around large cores. 72 points over 43 grains were analysed. Of these, 44 points were rejected due to observed discordance, Pb loss, and incorrect core-overgrowth age relationships. The remaining points came from overgrowths ($n = 5$) and cores ($n = 23$). The 5 results from overgrowths range between ~418–407 Ma and produced a weighted mean $^{206}Pb/^{238}U$ age of 412.0 ± 4.7 Ma (MSWD = 0.73) (Fig. 3). Of the cores, the youngest 18 points fell within the confidence interval of the overgrowth age. 5 older core spots fell between ~424–419 Ma, and a further 7 spots had individual ages of ~440, ~449, ~490, ~500, ~1430, and ~ 1450 (n = 2) Ma, respectively (Fig. 3). The weighted mean age of the overgrowths is interpreted as most likely representing magmatic emplacement, whilst the cores may include both antecrystic and xenocrystic growth.

4.1.4. Sample CR-05, NX 59450 98020

The sample is a granite of 0.1–3 mm grain size. Alkali feldspar dominates with lesser quartz, plagioclase and biotite, and accessory apatite and zircon. There is sericite and epidote after plagioclase and alteration of biotite to chlorite. Of 120 zircon grains mounted, 66 were imaged and 53 of these deemed suitable for laser ablation. Grains range from ~100–350 μm in length, are dominantly subhedral, and exhibit complex internal structures along with ubiquitous but variable amounts of fracturing and mineral inclusions. In most grains, cores are very large with smaller overgrowths. Most of the cores have complex shapes and are either un-zoned or contain faint oscillatory or sector zoning. Evidence of resorption is present in a few cores. The overgrowths typically exhibit faint oscillatory zoning with a few examples of sector zoning. All grains have a dark, un-zoned outermost layer of variable width, which for some grains represents the only overgrowth onto the core. 82 points over 53 grains were analysed for CR-05. Of these, 48 points were rejected due to observed discordance, Pb loss, and incorrect core-overgrowth age relationships. Of the remaining 34 concordant points, 13 overgrowths range in age between ~414–405 Ma, with a weighted mean $^{206}Pb/^{238}U$ age of 410.5 ± 1.8 Ma (MSWD = 0.78) (Fig. 3). Of 21 remaining zircon cores, 10 fell within the confidence interval of the overgrowths, 11 plotted between ~422–414 Ma, and a further two cores had individual $^{206}Pb/^{238}U$ ages of ~426 and ~ 427 Ma, respectively (Fig. 3). The weighted mean age of the overgrowths is interpreted as most likely representing magmatic emplacement, whilst the cores may mostly represent antecrystic growth. As the two oldest cores do not overlap in age with the termination of sedimentation in the Southern Uplands Accretionary prism, these are interpreted as potential xenocrysts.

4.2. Black Stockarton Moor and the Bengairn Pluton

4.2.1. Sample JD-01, Black Stockarton Moor phase 1 dyke, NX 70947 53015

The sample is a quartz diorite of 2–3 mm grain size, dominated by plagioclase with subordinate amphibole, quartz, and alkali feldspar, and accessory apatite, monazite, and zircon. There is replacement of feldspar with chlorite and calcite. Out of the 86 grains imaged, only 22 of these were suitable for analysis due to heavy fracturing and alteration. Most grains are subhedral and range from ~63–275 μm. The relative core to overgrowth size is variable, with complex internal structures including loss of zoning and extensive alteration most closely associated with fractures or inclusions. Where visible, zoning is oscillatory but patchy in the zircon cores. In most concordant grains, cores are rounded and the core to overgrowth boundary is clearly defined. In the discordant grains, the core to overgrowth boundary is more poorly defined, and cores are generally irregularly shaped. In concordant grains, most overgrowths contain heterogenous oscillatory or irregular zoning and occasionally faint sector zoning. Just 34 points were analysed over the 22 grains, 27 of these being omitted due to observed discordance, Pb loss, and incorrect core-overgrowth age relationships. The remaining 7 points came from cores ($n = 6$) plus one overgrowth. Together these points had a range of $^{206}Pb/^{238}U$ ages from ~424–416 Ma, and a weighted mean $^{206}Pb/^{238}U$ age of 419.1 ± 4.1 Ma (MSWD = 0.25) (Fig. 4).

4.2.2. Sample SM-02, Black Stockarton Moor phase 1 sheet; NX 72427 54975

This is a plagioclase-dominated quartz diorite of <0.1–2.5 mm grain size. There are smaller proportions of amphibole, quartz, and alkali feldspar with accessory apatite, titanite and zircon and secondary sericite, chlorite, and calcite. 70 zircon grains were mounted, with 21 suitable for laser ablation. Most analysed grains are ~75 – ~275 μm in length and subhedral. There is very poor definition of the core-overgrowth boundary, but cores generally appear to be larger than any overgrowths. Most analysed grains are unfractured and the sub-set of fractured grains often contain localised alteration. Where defined, cores in SM02 have complex shapes, some evidence of resorption, and are texturally heterogeneous with much sector zoning. Overgrowths typically contain patchy oscillatory zoning. 41 points over the 21 grains were analysed, and 27 omitted due to observed discordance, Pb loss, and incorrect core-overgrowth age relationships. Of the remaining 14 points, 3 were on definable overgrowths (1 on the outer part of an overgrowth, 2 on the inner part of overgrowths), together producing a weighted mean $^{206}Pb/^{238}U$ age of 407.8 ± 2.9 Ma (MSWD = 0.53) (Fig. 4). There were 11 acceptable points measured from zircon cores, with 5 of these plotting younger than or overlapping the weighted mean age above, possibly indicating a Pb loss issue. 6 further cores had ages ranging from 416 to 411 Ma and are plausibly antecrystic, or xenocrystic cores which experienced partial Pb loss (Fig. 4).

4.2.3. Bengairn Pluton, BG-01, NX 772 538

This rock is a quartz monzodiorite of <0.3–5 mm grain size, dominated by plagioclase, with subordinate alkali feldspar, amphibole, biotite, quartz and titanite. Accessory phases are apatite, titanite, zircon, and monazite. Secondary sericite, calcite, chlorite, and clays are present. 200 zircon grains were mounted for BG-01 but only 31 were suitable for laser ablation owing to extensive fracturing and alteration, perhaps associated with a fault striking parallel to Phase 2 of the Black Stockarton Moor intrusions (British Geological Survey, 1993). Zircons range from ~40–138 μm and are dominantly euhedral. Large cores and smaller overgrowths can be distinguished, the mostly euhedral cores showing irregular or patchy oscillatory or sector zoning with some evidence of resorption. The overgrowths display prominent oscillatory and occasional sector zoning. 59 points from these 31 grains were lasered, and 40 were omitted due to discordance, Pb loss, or incorrect core-overgrowth relationships. 6 points came from zircon overgrowths and defined a weighted mean $^{206}Pb/^{238}U$ age of 410.2 ± 1.7 Ma (MSWD = 1.4) (Fig. 4). Of 13 points from zircon cores, 8 plotted within or younger than the confidence interval of the overgrowth age. 5 further core ages lay between 423 and 413 Ma and are conceivably antecrystic, or xenocrysts which experienced partial Pb loss near the time of emplacement. A final point apparently pre-dates the termination of sedimentation in the accretionary prism, with an age of ~426 Ma, and is defined as xenocrystic (Fig. 4).

4.2.4. Sample SM-01, Black Stockarton Moor Phase 2 dyke; NX 73293 54509

This sample is a fine to medium grained quartz diorite of 0.1–2.5 mm grain size. Plagioclase dominates with minor amphibole, quartz, and alkali feldspar. Zircon is the only accessory phase. Sericite, chlorite, calcite, and epidote form the alteration assemblage. 65 grains were mounted but only 3 were identified as suitable for laser ablation, others being highly fractured, altered, or too complex and small for further analysis. Most grains are euhedral to subhedral with small cores and larger overgrowths, the core-overgrowth boundary being poorly defined. The three selected grains range from ~130–310 μm in length,

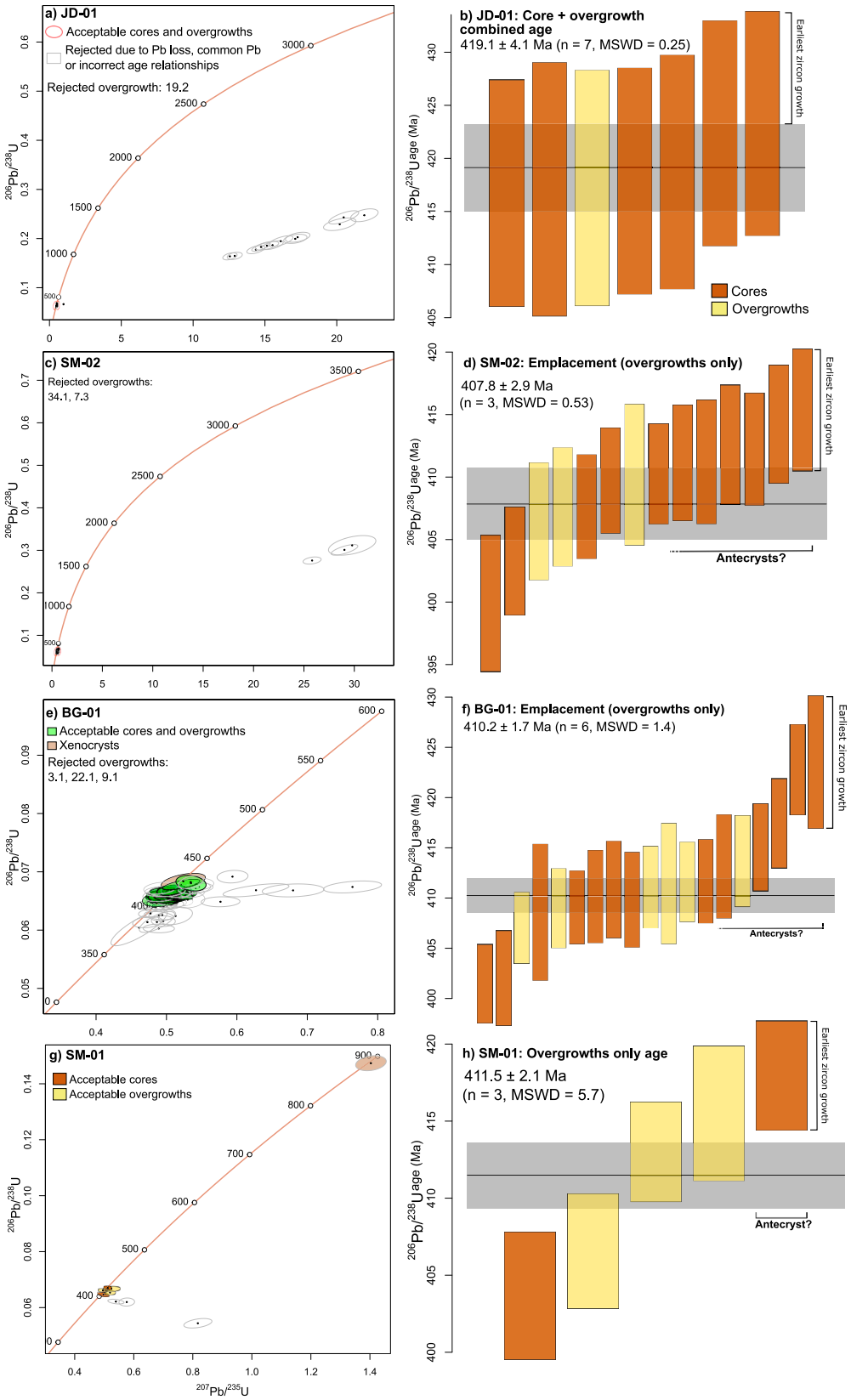

Fig. 4. Summary geochronological data for the Black Stockarton Moor sub-volcanic complex (a – d, g, h) and the Bengairn pluton (e, f). Symbology is clearly defined and may differ between plots.

but the others are smaller than these. Most cores in SM-01 are rounded, occasionally resorbed, and vary from having no to very faint oscillatory or irregular zoning. The overgrowths all have oscillatory zoning. 9 points from the 3 suitable grains were lasered, with 4 points omitted due to discordance. Of the 5 remaining points, 3 were from 2 successive overgrowths on the one grain, with individual point ages of 412.6 ± 3.2 Ma (outermost part of an outer overgrowth), 407.9 ± 3.7 Ma (inner part of the outer overgrowth), and 416.4 ± 4.4 Ma (earlier overgrowth nearer the core of the crystal). Two core points from other grains overlapped with these overgrowth ages, whilst the inherited core of the same grain had an age of ~890 Ma (Fig. 4).

4.3. Cheviot

4.3.1. Sample CH-01, NT 9369 2041

This sample is from the Standrop facies (Table 2), a quartz monzonite of 0.5–4 mm grain size, dominated by alkali feldspar with subordinate plagioclase, biotite, quartz, and tourmaline. Accessories include apatite and zircon. There is sericitisation of feldspars and replacement of biotite with chlorite, epidote, and clay. 117 zircons were mounted of which 54 were suitable for laser ablation. Most grains are subhedral, from ~95–350 μm in length, with distinctive cores and overgrowths. In most grains, the core is larger or of equal size to the overgrowths. Many of the grains are lightly fractured with alteration spatially related to those fractures, and there are many small inclusions throughout all grains. Cores in CH-01 vary from un-zoned to faintly zoned, with both oscillatory and sector zoning patterns. Most cores exhibit complex shapes and extensive resorption. Overgrowths are dominated by oscillatory zoning with some sector and convolute zoning also present. 97 points from the 54 grains were lasered but 61 of these were omitted due to discordance, Pb loss, or incorrect core-overgrowth relationships. Of the remaining 36 points, 9 came from overgrowths, producing a weighted mean $^{206}Pb/^{238}U$ age of 401.6 ± 4.3 Ma (MSWD = 0.44) (Fig. 5). Two of these points were visibly slightly older, albeit substantially overlapping with the other points on the weighted mean plot. Removing them from the weighted mean produces a revised age of 400.1 ± 4.7 Ma (MSWD = 0.25) (Fig. 5). 27 remaining points came from zircon cores, of which 21 are within the confidence interval of the overgrowth age, and 6 have ages ranging from ~417–407 Ma. The latter are antecrystic, or xenocrysts which may have experienced partial Pb loss at the time of

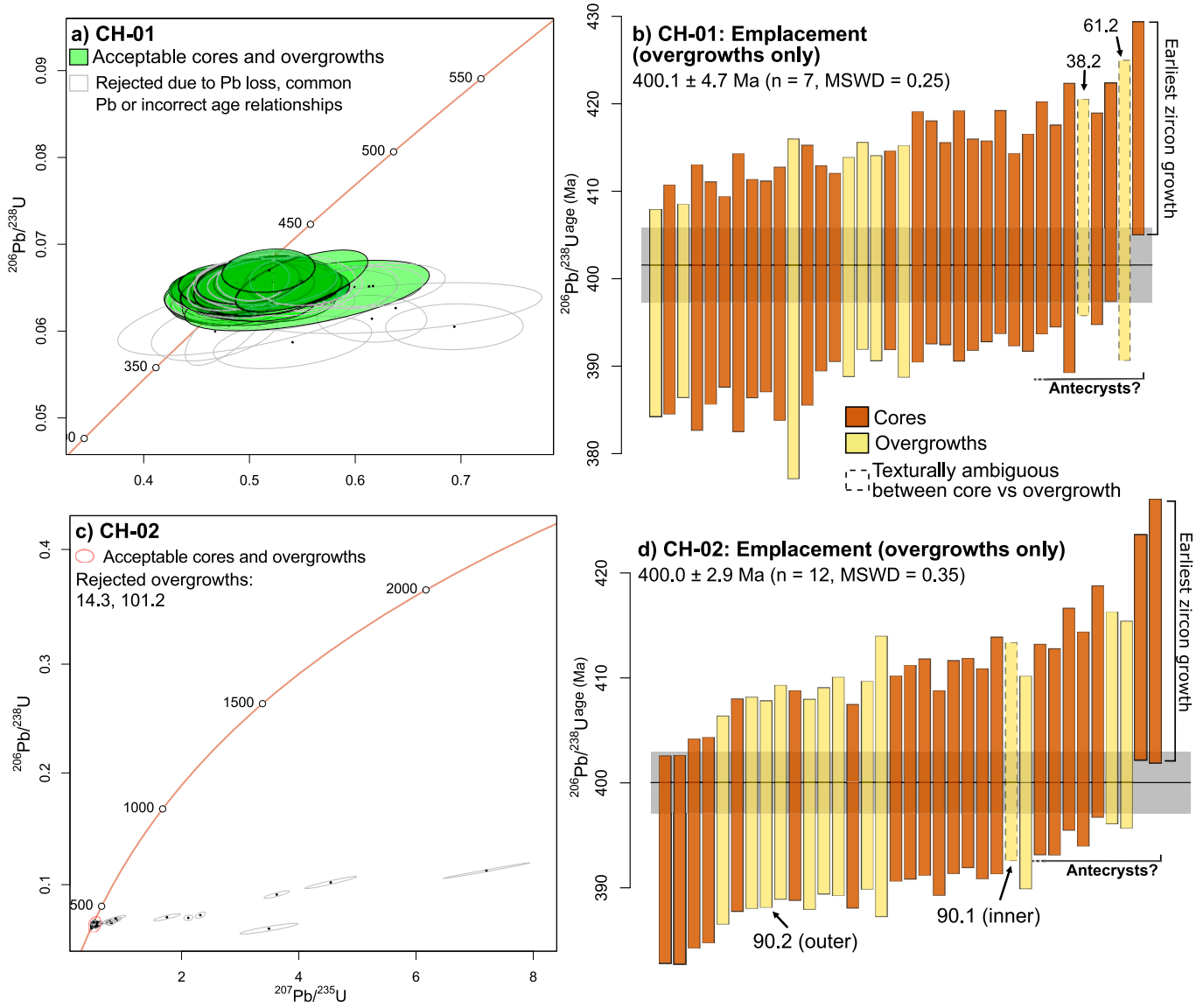

Fig. 5. Summary geochronological data for the Cheviot pluton. In b) points 38.2 and 61.2 are considered potentially antecrystic and are excluded from the final weighted mean age. In d) points 90.2 and 90.1 came from the outer and inner parts of an apparent overgrowth, with the inner age excluded from the final weighted mean.

emplacement (Fig. 5).

4.3.2. Sample CH-02, NT 9232 2047

This sample is from a northernly tributary of the Harthope river, part of the Hedgehope granophyre facies of Jhingran (1942) (Table 2). The rock is a syenogranite of 0.1–5 mm grain size, consisting dominantly of alkali feldspar, subordinate quartz, biotite and plagioclase and accessory apatite and zircon. There is sericitisation of feldspars and replacement of biotite with chlorite, epidote, and clay. The petrography of CH-02 is distinct from CH-01. 124 zircons were mounted for CH-02 of which 56 were suitable for laser ablation. Most grains are subhedral, ranging from ~150–300 μm in length. Cores and overgrowths are observed in most grains, though the relative core to overgrowth size varies. Most grains are very lightly fractured, with some associated alteration. Cores have complex shapes with few euhedral cores, and are mostly poorly zoned, through some faint oscillatory and sector zoning patterns are observed. The core-overgrowth boundaries are sometimes affected by alteration and resorption. Overgrowths are dominated by oscillatory zoning with some sector and convolute zoning also present. 92 points over 56 grains were analysed, with 57 points omitted due to Pb loss, discordance or incorrect core-overgrowth age relationships. Of the remaining 35 points, there were 13 overgrowths which provided a weighted mean $^{206}Pb/^{238}U$ age of 400.3 ± 2.8 Ma (MSWD = 0.34) (Fig. 5). Alternatively, by omitting 1 visually slightly older point from the innermost part of an overgrowth, a new weighted mean age of 400.0 ± 2.9 Ma (MSWD = 0.35) is produced (Fig. 5). The remaining 22 points were dominantly from cores and had ages broadly overlapping (n = 11) or even slightly younger (n = 4) than the overgrowths. Finally, 7 points had ages older

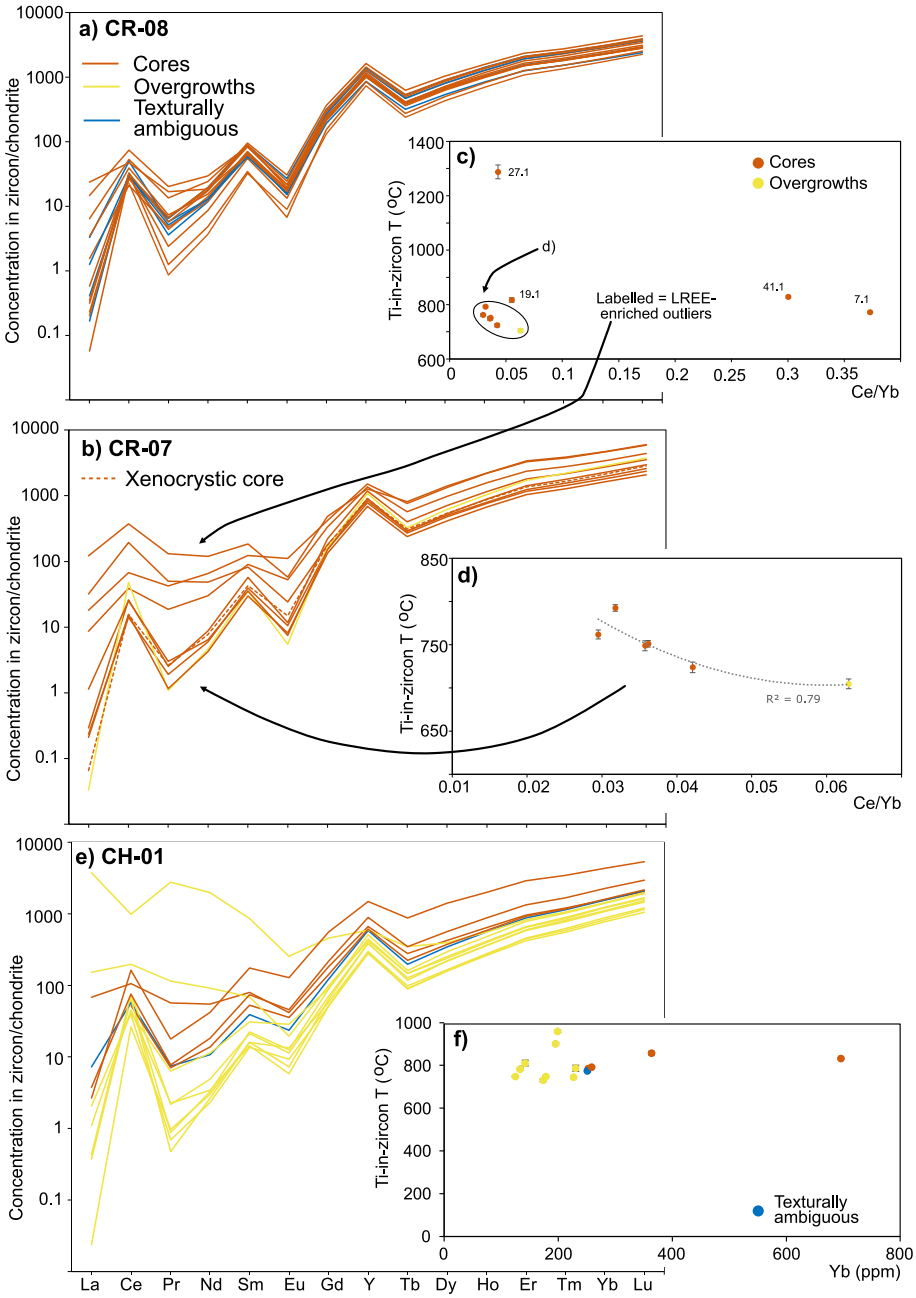

Fig. 6. Zircon trace element data for a - c) CR08 and d) CR07 (Carsphairn) and e-f) CH01 (Cheviot). REE data are normalised to the chondritic values of McDonough and Sun (1995). Error bars in b - c) and f) consider errors included in the Ti-in-zircon temperature equation of Watson et al. (2006) and errors associated with the measured Ti (ppm) concentration.

than the confidence interval of the overgrowths, ranging from ~415–403 Ma. These older cores are antecrystic, or xenocrysts which may have experienced partial Pb loss at the time of emplacement (Fig. 5).

4.4. Trace element data from Cairnsmore and Cheviot

4.4.1. Cairnsmore CR-08

Analyses from this sample are all from zircon cores. These mostly have steeply sloping REE patterns, from ~0.1–100 x chondritic values for the LREE to up to ~4000 x chondrite for the HREE, as well as prominent positive Ce and negative Eu anomalies (Fig. 6a). One spot has relative enrichment in the LREE, interpreted as partial interception of a LREE-enriched inclusion. The Ti-in-zircon temperatures of CR-08 cores range between ~851–753 °C with a mean of 805 ± 61 °C (2σ, $n = 14$). Two cores have significantly higher temperatures of ~909 °C and ~ 1020 °C, which may relate to ablation of LREE-enriched inclusions.

4.4.2. Cairnsmore CR-07

10 spots were analysed in CR-07, including 1 overgrowth and 9 cores, of which 1 with a $^{206}Pb/^{238}U$ age of ~425 Ma was assigned to be xenocrystic, though it has similar REE concentrations to other cores (Fig. 6b). The CR-07 overgrowth was LREE depleted and HREE enriched, with a Ti-in-zircon temperature of ~704 °C. CR-07 cores are generally LREE depleted (~0.2 x – 57 x chondritic values) and HREE enriched (up to ~2970 x chondritic values). All core and overgrowth spots exhibit positive Ce and negative Eu anomalies. Four core spots are LREE enriched (~8 x – 111 x chondritic values) compared to the rest of the dataset, again attributed to inclusions (Fig. 6b). The Ti-in-zircon temperatures of CR-07 cores generally range between ~723 °C – 828 °C, producing a mean Ti-in-zircon temperature of 774 ± 71 °C (2σ, $n = 8$) (Fig. 6c). One core has a significantly higher temperature of 1287 °C and correlates with a LREE enriched outlier. There is a strong negative correlation ($R^2 = 0.8$) between Ti-in-zircon temperature and chemistry (Fig. 6d).

4.4.3. Cheviot CH-01

Zircon analyses came from 9 overgrowths and 5 cores. The zircons mostly have steeply sloping REE patterns with prominent positive Ce anomalies as well as smaller negative Eu anomalies (Fig. 6e). Two overgrowths and one core have relative enrichment in the LREE. The remaining cores have typically higher REE concentrations than the overgrowths, with cores having LREE at ~2.5–175 x and rims at 0.01–75 x chondritic values, respectively. The cores have HREE at up to 5400 x and overgrowths up to 1700 x chondritic values. CH-01 cores have Ti-in-zircon temperatures of ~786–858 °C, producing a mean Ti-in-zircon temperature of 818 ± 68 °C (2σ, n = 4). whereas the overgrowths lie between ~731 °C – 961 °C ($n = 9$), with a mean of 803 ± 158 °C (2σ, n = 9) (Fig. 6f).

5. Discussion

5.1. Integrating zircon textures, ages, and chemistries

Across each of the locations studied, zircon cores appear to broadly overlap in single point ages with their overgrowths, albeit with a spread towards older ages in the former (Figs. 3–5). These older ages sometimes lie outwith the confidence interval of the weighted mean emplacement ages. The overlap in ages with the overgrowths does point towards substantial Pb loss from cores around the time of emplacement. As to the origin of the cores, one possibility is that the cores are broadly xenocrystic, with a variety of initial ages being overprinted due to substantial amounts of Pb loss, mostly around the time of emplacement. A second hypothesis is that most of the cores are antecrystic and related to earlier zircon growth within the magmatic system. Therefore, at least some of the older ages may retain geologically meaningful ages and relate to the timing of development of a lower crustal 'hot zone' prior to emplacement (e.g., Milne et al., 2023).

Excluding LREE-enriched zircon cores or overgrowths, there are relationships between zircon textures, chemistry, and temperatures (Fig. 6). We observe that zircon cores from Carsphairn and Cheviot, many of which have faint magmatic zoning, have very similar REE patterns to the overgrowths, albeit at slightly higher REE concentrations and Ti-in-zircon temperatures. The similar REE patterns imply that these cores are not derived from an unrelated magmatic system to that prevalent during overgrowth development. This interpretation favours an antecryst origin with cores formed at slightly higher temperatures when greater proportions of REE were available in the melt. Whole rock data are rather sparse in the Scottish Caledonides, but intrusions do tend to exhibit compatible behaviour of the REE during magma evolution (Milne et al., 2023). A general paucity of xenocryst populations is noted across the Southern Uplands (Hines et al., 2018; Miles et al., 2014), but where present, these have ages of >500 Myr (Hines et al., 2018). Hence, if our zircon cores were relict xenocrysts we would have expected at least some cores to be discordant, with Caledonian lower intercepts and ancient upper intercepts. More widely, magmatic zircons across the Southern Uplands-Down-Longford intrusions are also quite consistently younger than ~424 Ma, again difficult to reconcile with the cores being pre-collisional xenocrysts (Fig. 7). Therefore, we favour our second hypothesis that the zircon cores are mostly antecrystic. The logical conclusion from this interpretation is that the onset of magmatism deep within the accretionary prism does not pre-date ~424 Ma.

5.2. Local interpretation of the new U—Pb results

5.2.1. Carsphairn

Tindle et al. (1988) argued on geochemical grounds that Carsphairn was emplaced in 4 stages, starting with the outermost quartz diorite (CR08, our date only from zircon cores of 413.8 ± 1.2 Ma), evolving by fractionation to the inner granodiorite (CR07, our date 415.3 ± 1.7 Ma), and overprinted by a more evolved melt, producing the inner fine-grained granite (CR06, our date from zircon overgrowths 412.0 ± 4.7 Ma) then the innermost coarse-grained granite (CR05, our date from zircon overgrowths 410.5 ± 1.8 Ma). Whilst two of our ages based on overgrowths are within analytical error of each other, CR07 is inconsistent with field relations and Tindle et al.'s petrogenetic interpretation, instead overlapping with the original Rb—Sr data of Thirlwall et al. (1988). The older age had a higher MSWD than other samples, thus may not be accurate and instead could represent contribution from a deeper crustal mush, as argued for the nearby Doon pluton (Hines et al., 2018). Modest Ti-in-zircon temperatures would indicate near-solidus zircon growth, potentially supporting this hypothesis (Fig. 6). The final emplacement age can only be confidently defined based on the two youngest results from zircon overgrowths, to ~412–411 Ma; nevertheless, substantially older than the ~397 Ma age of the nearby Doon pluton. These results potentially indicate a long history of transtension on the Leadhills Fault (see Hines et al., 2018).

5.2.2. Black Stockarton Moor and Bengairn

Because of their fine grain size and intermediate compositions, it is probable that analysed zircons from Black Stockarton Moor are antecrystic, whereas zircon overgrowths at Bengairn are more likely to represent emplacement. Field evidence indicates that emplacement occurred in the order JD-01 > SM-02 > BG-01 > SM-01. The age of JD-01 of ~419 Ma came entirely from zircon cores, representing a maximum emplacement age. The ages from zircon overgrowths from SM-02 and BG-01 of ~408 and ~ 410 appear in the wrong order based on field evidence, though there is overlap between the ages. It is not possible to definitively date SM-01 (Section 4.2.4). Overall, magmatism occurred from as early ~424 Ma based on the oldest zircon cores analysed in JD-01 and BG-01 and likely finished by ~408 Ma. Miles et al. (2014) included the Bengairn pluton within the Criffell-Dalbeattie body

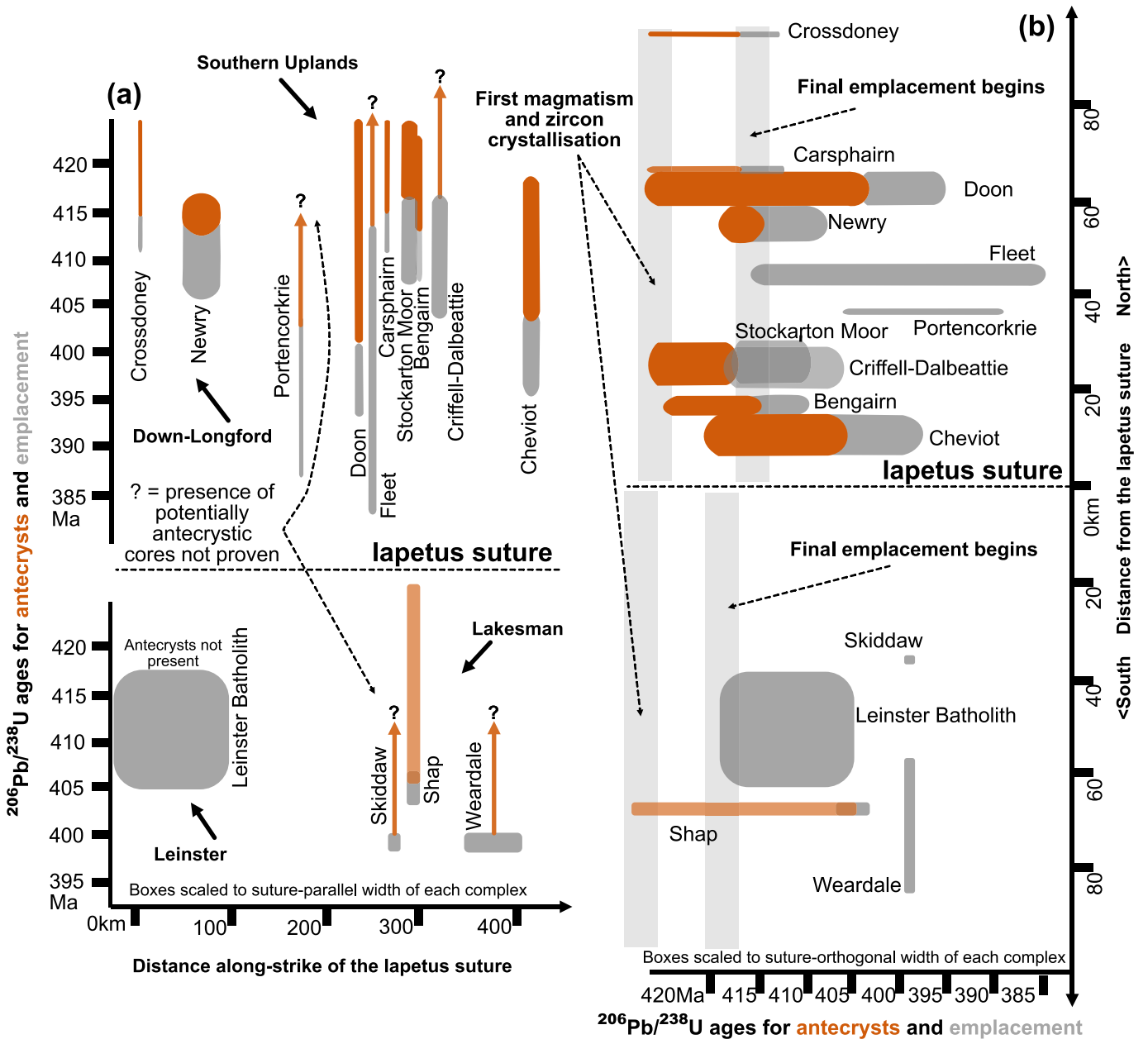

Fig. 7. Emplacement ages and ranges of earlier zircon growth based on published U-Pb data from the Southern Uplands-Down-Longford and Leinster-Lakesman terranes, relative to a) distance along the Iapetus suture zone from west to east and b) distance to the north or south of the Iapetus suture. Note that the ages for Crossdoney are based on $^{206}Pb/^{238}U$ results in preference to Fritschle (2016)'s $^{206}Pb/^{207}Pb$ data. Data sources are listed in Table 1 and the main text.

as its outermost Zone 1, to which they assigned a weighted mean $^{206}Pb/^{238}U$ ion microprobe age of 408 ± 14 Ma (n = 9). The date for Zone 1 in Miles et al. (2014) was collected from the far north of the Criffell pluton, ~20 km northeast of the proposed contact with the Bengairn pluton, and still further from our sampled location with an age of 410.2 ± 1.7 Ma. Overall, magmatic activity in this cluster of bodies appears to have lasted at least ~15 Myr, but isotope dilution methods on zircons and probably Rb—Sr on micas would help remove ambiguity over the duration of magmatism in this area.

5.2.3. *Cheviot*

Petrographic distinction between the samples confirms that CH-01 and CH-02 are from different facies (Jhingran, 1942). That said, the samples present very similar zircon populations, and our new ages overlap with existing Rb—Sr data for the pluton and the volcanic complex (Thirlwall, 1988). Both weighted mean ages could be improved with longer counting times or isotope dilution methods with the aim of determining the total timeframe of emplacement. The oldest zircon cores date to ~417 Ma, confirming, as with the other locations, that magmatism commenced deep within the crust millions of years prior to emplacement. Cheviot has previously been associated with minor epithermal and porphyry-type enrichment in Cu, Mn, Ba, Pb, Zn and U mineralisation (Cameron et al., 1988) and is marginally high heat producing (McCay and Younger, 2017), so further assessment of the applied value of this granite is merited.

5.3. *Magmatism and Iapetus closure: towards a consistent geodynamic model*

There are many different interpretations for the tectonic setting of magmatism in the Southern Uplands, Midland Valley and Grampian Highlands of Scotland, as well as much debate over the tectono-

stratigraphy of the Southern Uplands, aptly summarised in Stone (2024) and Law et al. (2024). Past work has typically related magmatism north of the suture to north-dipping Iapetus subduction beneath the Laurentian margin, stretching from the end of the Grampian Orogeny until terminal Avalonia-Laurentia collision (e.g., Oliver et al., 2008; Thirlwall, 1982). Crustal transtension has also been implicated in magmatism (Brown et al., 2008; Dewey and Strachan, 2003; Hines et al., 2018; Miles et al., 2014), as well as debated roles for lithospheric delamination (e.g., Freeman et al., 1988; O'Reilly et al., 2012), and under-thrusting of peri-Gondwanan lithosphere (Miles et al., 2014; Stone, 2024 and references therein).

The timing of collision and the timing and effect of Iapetus slab breakoff are especially problematic. Various authors (e.g., Archibald et al., 2022; Archibald and Murphy, 2021; Hines et al., 2018; Miles et al., 2016) envisage break-off at ~430 Ma, meaning all the magmatism has a post-subduction timing (e.g., Richards, 2009). A ~ 430 Ma breakoff event, prior to the end of sedimentation in the accretionary prism seems inconsistent with the typical occurrence of breakoff some millions of years after continental collision begins (c.f. Van Hunen and Allen, 2011). This dichotomy indicates a need to determine how much of the stratigraphy of the Southern Uplands-Down-Longford terranes relates directly to subduction-accretion, and whether sedimentation continued even after the onset of continental collision.

At the other temporal extreme, Oliver et al. (2008) argued for an episode of divergent double subduction lasting until ~400 Ma beneath terranes north and south of the Iapetus suture. Oliver et al. (2008) proposed simultaneous break-off of the Iapetus slabs at ~400 Ma. This timing implies that the bulk of magmatism must have been generated in a continental arc above an Iapetus subduction zone. This scenario presents issues too: it requires an almost non-existent arc-trench gap, assuming the modern-day position of the prism relative to the suture is reflective of its Palaeozoic configuration. Initial magmatism beneath Cheviot directly over the Iapetus suture at ~417 Ma also requires the absence of a slab by that time, not by ~400 Ma (the latter based on the final emplacement ages). Additionally, there is no clear evidence for a south-dipping suture zone beneath northern England to confirm the double subduction model.

There is a further conundrum: the origin of extensive magmatism south of the Iapetus suture across the Leinster-Lakesman terrane (Fig. 7), especially if not related to south-dipping subduction as envisaged by Oliver et al. (2008). There is remarkable temporal overlap between the Southern Uplands-Down-Longford data and emplacement of the Leinster batholith of Ireland from ~417–405 Ma (U—Pb zircon ion probe emplacement ages; (Fritschle et al., 2018). Zircon ion probe dating combined with Re—Os sulfide data reveal magmatism beneath Shap, Northern England to have started no earlier than about ~428 Ma (based on a single zircon), with final emplacement of the Shap pluton at ~405 Ma (Miles and Woodcock, 2018; Selby et al., 2008). Further Re—Os data indicate emplacement of the Skiddaw pluton and Weardale batholith at ~399–398 Ma (Selby et al., 2008), the latter confirmed with a U—Pb zircon isotope dilution concordia age of 399 ± 1 Ma (Kimbell et al., 2010) (Fig. 7). Miles et al. (2016) proposed that a ~ 430 Ma Iapetus slab break-off affected mantle dynamics for ~100 km north and south of the Iapetus suture, resulting in a wide area of mantle upwelling and tens of millions of years of mafic melt addition into the lower crust.

5.3.1. *Zircon growth vs the timing of emplacement: a relationship to slab dynamics beneath the Laurentian margin?*

Our new U—Pb zircon ages have some bearing on these proposed geodynamic solutions, as they establish more clearly the times at which magmatism began deep beneath the Southern Uplands (~424 Ma) and when emplacement events started to occur (~415 Ma).

Results are compiled from across the Southern Uplands-Down Longford and Leinster-Lakesman terranes (Fig. 7). These data show us that magmatism started no earlier than ~428 Ma, based on one grain from the Shap granite, but more typically no earlier than ~424 Ma, regardless of when final emplacement occurred (Fig. 7; Fritschle et al., 2018; Miles and Woodcock, 2018). Spatially, there is no relationship between the onset of magmatism and distance along the Iapetus suture (Fig. 7a), nor is there much temporal relationship vs distance for 100 km north or south of the suture (Fig. 7b). The oldest zircon cores at Cheviot can only provide a minimum age of the onset of magmatism at the suture of ~417 Ma.

Looking further north in the collision zone, there has been little research on antecrystic zircons in magmatism of the Midland Valley or Grampian Highlands of Scotland. However, at this broader scale of up to 250 km from the Iapetus suture, emplacement ages do show a clear southward-younging pattern (Law et al., 2024). Emplacement began at ~432 Ma in the north of the Grampian Terrane (Auldearn granite, 432 ± 10 Ma, U—Pb zircon ion probe; Oliver et al., 2008), at ~424 Ma in the Midland Valley (Sidlaw Hills, 423.6 ± 6.1 Ma, Rb-Sr (Thirlwall, 1988), and finally at ~415 Ma in the accretionary complex (Table 1). No emplacement occurred before ~417 Ma to the south of the Iapetus suture (Fig. 7).

Our interpretation of these ages is that, by ~424 Ma, the Iapetus slab had accelerated its rollback, moving the zone of active mantle wedge melting southwards from beneath the Grampian Highlands and the Midland Valley, to beneath the accretionary complex. Ultimately, the trigger for accelerated rollback would be the onset of continental collision at the Laurentian margin (Fig. 8a; Baumann et al., 2010). This process would enable the onset of magmatic activity, resulting in the first zircon crystallisation in the lower crust of the accretionary complex by ~424 Ma. Crustal compression at this time would likely prevent final emplacement of magmas into the shallower crust.

The slab would have to have broken off, or at least the lithosphere been significantly thinned beneath the suture for magmatism to commence beneath Cheviot by a minimum age of ~417 Ma. Based on our results, we suspect a timing of ~428–424 Ma could be appropriate for slab breakoff. This timing is geologically consistent in postdating Miles et al.'s (2016) proposed onset of collision, but pre-dating any magma generation north and south of the Iapetus suture, particularly on the suture itself at Cheviot. That said, we note that slab break-off has for some time been an unquestionably popular model to explain Caledonian collision magmatism (Atherton and Ghani, 2002; Neilson et al., 2009). The model has recently been criticised in terms of its timing, applicability far from the suture, and the geochemical similarity of associated magmatism to 'normal' continental arcs (Law et al., 2024). Geodynamic modelling now demonstrates that breakoff is a deep geodynamic feature only linked directly to spatially limited, small volume magmatism at the suture (e.g., Freeburn et al., 2017). In contrast to Miles et al. (2016), we accordingly view breakoff as just one part of the collision process, not a full explanation for the occurred of magmatism both north and south of the Iapetus suture. Following breakoff, in our view, lithospheric thinning should also play a significant role in magmatism (e.g., Neill et al., 2015; Fig. 8b). A possible analogue occurs in Arabia-Eurasia collision zone, where Late Cenozoic magmatism across Iran, the Caucasus and Turkey substantially post-dates breakoff events (Neill et al., 2015). Magmatism extends south of the Bitlis-Zagros suture within the lower plate (Arabia) in the form of Karacadag volcano (Neill et al., 2015; Pearce et al., 1990), in the same position relative to the suture as the Leinster-Lakesman intrusions. Magmatism either side of the suture has been attributed to delamination of lithosphere weakened by subduction processes millions of years prior to the present (Neill et al., 2015; Pearce et al., 1990). One way of testing this model would be via the geochemistry of mafic enclaves or minor intrusions, identifying if the mantle component of magmatism within the Leinster-Lakesman terrane was broadly of within-plate (non-subduction) character.

Furthermore, our data show that final emplacement events occurred some 10–30 Myr after the proposed timing of breakoff, lasting considerably longer than its modelled short-lived effects on mantle dynamics (Freeburn et al., 2017). The onset of emplacement at ~415 Ma much better correlates with the onset of regional transtension than breakoff,

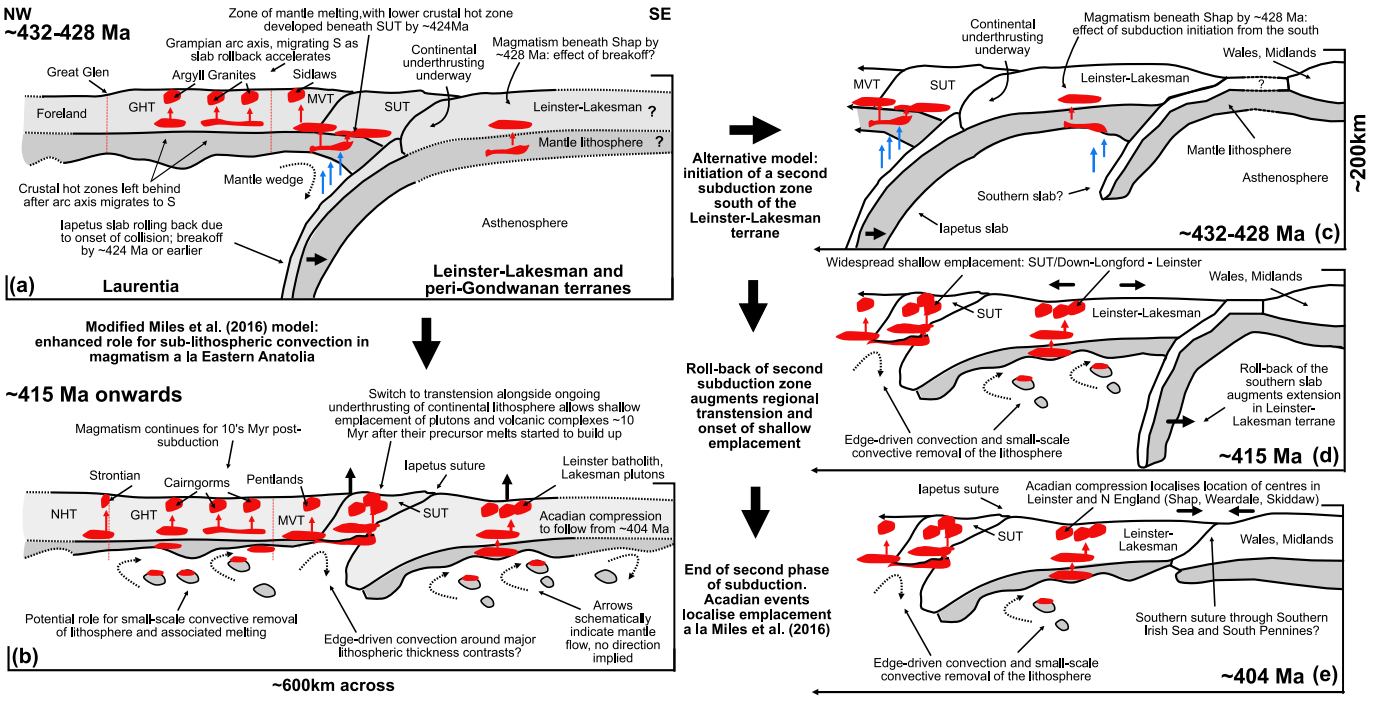

Fig. 8. Geodynamic interpretations of the Caledonian-Acadian belt in Scotland, England, Wales and Ireland. The basis of the model is adapted from the reconstruction of Miles et al. (2014) and the geodynamic models of Baumann et al. (2010). a) Roll-back of the Iapetus slab as the Leinster-Lakesman lithosphere begins to collide with the Laurentian continental margin. b) Further under-thrusting of continental lithosphere triggers uplift and transpression, coupled with wider lithospheric thinning and sub-lithospheric convection. In c), we indicate how the onset of magmatism beneath the Leinster-Lakesman terrane could instead be related to a second subduction zone. d) Slab rollback augments regional transtension. e) Terminal collision results in the Acadian Orogeny and the final localised emplacement of magmas in the Leinster-Lakesman terrane. GHT = Grampian Highlands Terrane; MVT = Midland Valley Terrane; NHT = Northern Highlands Terrane; SUT = Southern Uplands Terrane.

the former permitting remobilisation of long-stored lower crustal mushes (Fig. 8b; Brown et al., 2008).

5.3.2. *Pluton chemistry and its relationship to subduction, collision and transtension*

Critical to this revised timescale of geodynamic events north of the Iapetus suture is that the onset of magmatism was due in the first instance to mantle melting processes which can be directly attributed to subduction dynamics. Whilst melting of typical crustal lithologies leads to the generation of partial melts with $SiO_2 > 60$ wt% (Rapp et al., 1991; Rapp and Watson, 1995; Wolf and Wyllie, 1994), samples from Carsphairn, Doon, and Newry are all are more mafic than this, and are therefore likely to be mantle derived (Anderson et al., 2016; Brown et al., 1979b; Cooper et al., 2016; Hines et al., 2018; Tindle et al., 1988). Analysis of elemental and isotopic data for Southern Uplands plutons also emphasises mantle-like trace element ratios, allied to a role for crustal assimilation during petrogenesis (Hines et al., 2018). Sr/Y ratios, sensitive to different depths of differentiation, have been used to argue for moderate crustal thicknesses of <45 km at the time of magmatism (Hines et al., 2018), much thinner than present-day orogens where crustal melting is a dominant process, such as the core of the Himalayas (England and Thompson, 1986).

That said, there is also a considerable body of geochemical evidence, including Rb—Sr, Lu—Hf, and Pb isotope studies, for melting of underthrust crust as collision proceeded (Brown et al., 2008; Halliday et al., 1980; Halliday et al., 1985; Halliday and Stephens, 1984; Miles et al., 2014; Soper et al., 1992; Stone et al., 2012); Fig. 8b). Under-thrusting would proceed to eliminate the mantle wedge beneath the suture and generally suppress mantle melting with time (e.g., Magni et al., 2017). We envisage that hybridisation processes would occur in a lower crustal hot zone between lower plate partial melts, and earlier stored mantle-derived mushes, resulting in the range of zircon ages and the geochemistry of the emplaced bodies. The under-thrusting of buoyant continental lithosphere could potentially explain the origin of regional transtension from ~415 Ma, as the buoyant lithosphere would eventually be unable to penetrate deeper into the mantle, especially without the effect of slab pull forces from ~424 Ma.

5.3.3. *Trans-suture magmatism: beyond slab breakoff?*

Having justified a modification of the Miles et al. (2016) model to downplay the role of slab breakoff in magmatism, we also explore an alternative testable explanation for the presence of magmatism on the southern side of the Iapetus suture (Figs. 8c-e).

In this model, magmatism north and south of the Iapetus suture are not directly related to each other. Hitherto unpublished work (e.g., Waldron et al., 2024) has recently implied the presence of a second suture, referred to as the Môn Line, broadly parallel to the Iapetus suture but to the south of the Leinster-Lakesman terrane. We envisage in Figs. 8c-e that magmatism of the Leinster-Lakesman terrane could have resulted from a separate short-lived phase of north-dipping subduction. Subduction would have begun shortly prior to ~428 Ma (age of the oldest magmatic zircon at Shap; Miles and Woodcock, 2018), plausibly triggered by the onset of collision between the Leinster-Lakesman terrane and the Laurentian margin further north (Fig. 8c). The onset of regional transtension, concurrent with emplacement of the early components of the Leinster batholith (Fritschle et al., 2018), may have been augmented by rollback of the southerly Iapetus slab (Fig. 8d). Subduction would have ended with the Acadian orogeny at ~404 Ma (Waldron et al., 2024), with magmatism in the Leinster-Lakesman terrane accordingly dying out a few Myr later (Fig. 8e). As with the single subduction zone model (Figs. 8a-b), geochemistry of mafic magmatic components may play an important role in identifying subduction-related origins. However, additional geophysical examination of the deep crust along the proposed Môn Line would be merited.

6. Conclusions and recommendations for further research

This study focused first on the Palaeozoic Southern Uplands-Down-Longford terranes, an accretionary complex on the Laurentian margin of the Iapetus Ocean, before broadening out to explore the wider implications of magmatism across the Iapetus suture. The prism contains magmatic bodies associated with collision between the margin and allochthonous terranes. Our new U—Pb zircon age constraints allow us to better constrain the magmatic record and its association with geodynamic processes.

1) The complexes we have analysed for this study contain zircon cores which grew prior to final emplacement. Magmatism beneath much of the accretionary complex did not start prior to ~424 Ma. By considering the total zircon history, we can attribute the onset of magmatism to accelerated rollback of the Iapetus slab following the onset of continental collision at the Laurentian margin. A time of ~428–424 Ma is interpreted as a best estimate for slab breakoff.
2) Final emplacement of magmatic bodies north of the Iapetus Suture is recorded by magmatic zircon overgrowths and via Rb—Sr studies (e.g., Thirlwall, 1988). Shallow crustal emplacement did not commence until 415 Ma. Emplacement involved remobilisation of existing batches of magma from the lower crust as well as further magmatic additions from the accretionary complex and under-thrust continental lithosphere. The key driver of emplacement was likely to have been regional transtension (Fig. 8b, d).
3) Geodynamic reconstructions need to explain penecontemporaneous magmatism on either side of the Iapetus Suture. We are not convinced that breakoff plays a significant role in magmatism, counter to earlier popular models (Atherton and Ghani, 2002; Law et al., 2024; Neilson et al., 2009), including the reconstruction of Miles et al. (2016). We consider the possible role of broader lithospheric delamination and small-scale convection processes (Fig. 8a-b), as well as a new subduction configuration involving two separate slabs (Waldron et al., 2024; Fig. 8c-e).
4) Our new ages, though contributing to knowledge of the Southern Uplands and collision magmatism more widely, could be improved via additional zircon pre-treatment, multi-collector laser ablation, ion probe studies, and potentially sequential dissolution of complex zircon grains prior to thermal ionisation mass spectrometry. A fuller study of zircon trace element data as well as O and Lu—Hf isotopes across emplacement-related, antecrystic, and rare xenocrystic zones would be hugely helpful in constraining the temporal evolution of magma sources. Such research is plainly also necessary for magmatism of the Midland Valley and particularly the Grampian Highlands, representing the main Caledonian arc axis. The latter is increasingly of interest regarding mineral prospectivity and deep geothermal energy sources (McCay and Younger, 2017).

Funding

Data were generated with financial assistance from the Lord Kelvin - Adam Smith Fellowship of the University of Glasgow to JFE (project number 246866-01) and a research incentive grant from the School of Geographical and Earth Sciences of the University of Glasgow to IN (project number 126438-01).

CRediT authorship contribution statement

Chloe A.R. Gemmell: Writing – review & editing, Writing – original draft, Validation, Methodology, Investigation, Formal analysis, Data curation. **Iain Neill:** Writing – review & editing, Writing – original draft, Supervision, Software, Resources, Project administration, Methodology, Investigation, Funding acquisition, Data curation, Conceptualization. **Mark Wildman:** Supervision, Methodology, Formal analysis, Data curation. **Careen MacRae:** Methodology, Investigation, Formal analysis, Data curation. **David Currie:** Supervision, Investigation, Conceptualization. **Joshua F. Einsle:** Investigation, Funding acquisition.

Declaration of competing interest

The authors declare the following financial interests/personal relationships which may be considered as potential competing interests:

IN serves on the wider Editorial Board of Lithos but has published in the journal as lead or corresponding author only twice, in 2010 and 2013. Other authors declare that they have no known competing financial interests or personal relationships that could have appeared to influence the work reported in this paper.

Acknowledgements

This work forms part of the MSc by Research projects of CG and CM. We gratefully acknowledge Liene Spruženiece of the Geoanalytical Electron Microscopy and Spectroscopy facility at the University of Glasgow for training and instrument time. IN has in various ways been influenced by discussion and readings from Ed Stephens, Dan Barfod, Tobias Fritschle, Darren Mark, Andrew Miles, Julian Pearce, Rob Strachan, and Matthew Thirlwall. We thank Fernando Corfu and an anonymous reviewer for detailed comments which substantially improved this article. DC publishes with permission of the British Geological Survey.

References

Al-Hafdh, N.M.S., 1985. The Alteration Petrology of the Cheviot Granite. Unpublished PhD thesis,. Newcastle University, p. 347.
Anderson, P.E., Cooper, M.R., Stevenson, C.T., Hastie, A.R., Hoggett, M., Inman, J., Meighan, I.G., Hurley, C., Reavy, R.J., Ellam, R.M., 2016. Zonation of the Newry Igneous complex, Northern Ireland, based on geochemical and geophysical data. Lithos 260, 95–106.
Annen, C.J., Blundy, J.D., Sparks, R.S.J., 2006. The genesis of intermediate and silicic magmas in deep crustal hot zones. J. Petrol. 47, 505–539.
Archibald, D.B., Murphy, J.B., 2021. A slab failure origin for the donegal composite Batholith, Ireland as indicated by trace-element geochemistry. In: Murphy, J.B., Strachan, R.A., Quesada, C. (Eds.), Geological Society of London Special Publications 503, pp. 347–370.
Archibald, D.B., Murphy, J.B., Fowler, M., Strachan, R.A., Hildebrand, R.S., 2022. Testing petrogenetic models for contemporaneous mafic and felsic to intermediate magmatism within the "newer granite" suite of the Scottish and Irish Caledonides. In: Kuiper, Y.D., Murphy, J.B., Nance, R.D., Strachan, R.A., Thompson, M.D. (Eds.), New Developments in the Appalachian-Caledonian-Variscan Orogen, Geological Society of America Special Paper, vol. 554, pp. 375–399.
Atherton, M.P., Ghani, A.A., 2002. Slab breakoff: a model for Caledonian, late granite syn-collisional magmatism in the orthotectonic (metamorphic) zone of Scotland and Donegal, Ireland. Lithos 62, 65–85.
Badenszki, E., Daly, J.S., Whitehouse, M.J., Kronz, A., Upton, B.G.J., Horstwood, M.S.A., 2019. Age and Origin of Deep Crustal Meta-igneous Xenoliths from the Scottish Midland Valley: Vestiges of an Early Palaeozoic Arc and 'Newer Granite Magmatism. J. Petrol. 60, 1543–1574.
Baumann, C., Gerya, T., Connolly, D., 2010. Numerical modelling of spontaneous slab breakoff dynamics during continental collision. In: Spalla, M.I., Marotta, A.M., Gosso, G. (Eds.), Advances in Interpretation of Geological Processes: Refinement of Multi-Scale Data and Integration in Numerical Modelling, vol. 332. Geological Society of London Special Publication, pp. 99–114.
Bird, A.F., Thirlwall, M.F., Strachan, R.A., Manning, C.J., 2013. Lu–Hf and Sm–Nd dating of metamorphic garnet: evidence for multiple accretion events during the Caledonian Orogeny in Scotland. J. Geol. Soc. Lond. 170, 301–317.
British Geological Survey, 1993. Dalbeattie. Geological Survey of Scotland, 1:63,360/1: 50,000 (geological map series.).
Brown, M.J., Leake, R.C., Parker, M.E., Fortey, N.J., 1979a. Porphyry Style Copper Mineralisation at Black Stockarton Moor, South-West Scotland. Mineral Reconnaissance Programme Report. Institute of Geological Sciences, p. 100.
Brown, G.C., Cassidy, J., Tindle, A.G., Huges, D.J., 1979b. The loch doon granite: an example of granite petrogenesis in the British Caledonides. J. Geol. Soc. Lond. 136, 745–753.
Brown, P.E., Ryan, P.D., Soper, N.J., Woodcock, N.H., 2008. The newer granite problem revisited: a transtensional origin for the early Devonian trans-suture suite. Geol. Mag. 145, 235–256.
Cameron, D.G., Cooper, D.C., Bide, P.J., Allen, P.M., Haslam, H.W., 1988. A Geochemical Survey of Part of the Cheviot Hills and Investigations of Drainage Anomalies in the Kingsseat Area. Unpublished report. British Geological Survey, Keyworth, Nottingham, p. 23.

Chew, D.M., Strachan, R.A., 2014. The Laurentian Caledonides of Scotland and Ireland. In: Corfu, F., Gasser, D., Chew, D.M. (Eds.), Geological Society, vol. 390, pp. 45–91. London, Special Publications.
Chiaradia, M., 2022. Distinct magma evolution processes control the formation of porphyry Cu-au deposits in thin and thick arcs. Earth Planet. Sci. Lett. 599, 117864.
Cooper, M., Anderson, P., Condon, D., Stevenson, C., Ellam, R., Meighan, I., Crowley, Q., 2016. Shape and Intrusion history of the late Caledonian Newry Igneous complex, Northern Ireland. In: Young, M. (Ed.), Unearthed: Impacts of the Tellus Surveys of the North of Ireland. Royal Irish Academy book series, Dublin, pp. 145–156.
Couzinié, S., Laurent, O., Moyen, J.-F., Zeh, A., Bouilhol, P., Villaros, A., 2016. Post-collisional magmatism: crustal growth not identified by zircon Hf-O isotopes. Earth Planet. Sci. Lett. 456, 182–195.
Dewey, J.F., Strachan, R.A., 2003. Changing Silurian–Devonian relative plate motion in the Caledonides: sinistral transpression to sinistral transtension. J. Geol. Soc. Lond. 160, 219–229.
Dewey, J.F., Dalziel, I.W.D., Reavy, R.J., Strachan, R.A., 2015. The neoproterozoic to mid-devonian evolution of Scotland: a review and unresolved issues. Scott. J. Geol. 51, 5–30.
England, P.C., Thompson, A., 1986. Some thermal and tectonic models for crustal melting in continental collision zones. In: Coward, M.P., Ries, A.C. (Eds.), Collision Tectonics, Geological Society of London Special Publications, vol. 19, pp. 83–94.
Evans, J.A., 1995. Geochronology. In: Stone, P. (Ed.), Geology of the Rhins of Galloway. District Memoir of the British Geological Survey, Sheets 1 and 3 (Scotland). Her Majesty's Stationery Office, London, UK, p. 96.
Freeburn, R., Bouilhol, P., Maunder, B., Magni, V., van Hunen, J., 2017. Numerical models of the magmatic processes induced by slab breakoff. Earth Planet. Sci. Lett. 478, 203–213.
Freeman, B., Klemperer, S.L., Hobbs, R.W., 1988. The deep structure of northern England and the Iapetus Suture zone from BIRPS deep seismic reflection profiles. J. Geol. Soc. Lond. 145, 727–740.
Fritschle, T.J., 2016. Age and Origin of Late Caledonian Granites and Ordovician Arc Magmatic Rocks in Ireland and the Isle of Man. Unpublished PhD thesis,. University College Dublin, p. 379.
Fritschle, T.J., Daly, J.S., Whitehouse, M.J., McConnell, B., Buhre, S., 2018. Multiple intrusive phases in the Leinster Batholith, Ireland: geochronology, isotope geochemistry and constraints on the deformation History. J. Geol. Soc. Lond. 175, 229–246.
Halliday, A.N., Stephens, W.E., 1984. Crustal controls on the genesis of the 400 Ma old Caledonian granites. Phys. Earth Planet. Inter. 35, 89–104.
Gómez-Frutos, D., Castro, A., Gutiérrez-Alonso, G., 2023. Post-collisional batholiths do contribute to continental growth. Earth Planet. Sci. Lett. 603, 117978.
Halliday, A.N., Stephens, W.E., Harmon, R.S., 1980. Rb-Sr and O isotopic relationships in 3 zoned Caledonian Granitic Plutons, Southern uplands, Scotland: evidence for varied sources and hybridization of magmas. J. Geol. Soc. Lond. 137, 329–348.
Halliday, A.N., Stephens, W.E., Hunter, R.H., Menzies, M.A., Dickin, A.P., Hamilton, P.J., 1985. Isotopic and chemical constraints on the building of the deep Scottish lithosphere. Scott. J. Geol. 21, 465–491.
Hines, R., Paterson, S.R., Memeti, V., Chambers, J.A., 2018. Nested incremental growth of zoned upper crustal Plutons in the Southern Uplands Terrane, UK: fractionating, mixing, and contaminated magma fingers. J. Petrol. 59, 483–516.
Jhingran, A.G., 1942. The Cheviot granite. Q. J. Geol. Soc. Lond. 98, 241–259.
Keskin, M., 2003. Magma generation by slab steepening and breakoff beneath a subduction-accretion complex: an alternative model for collision-related volcanism in Eastern Anatolia, Turkey. Geophys. Res. Lett. 30. https://doi.org/10.1029/2003GL018019.
Kimbell, G.S., Young, B., Millward, D., Crowley, Q.G., 2010. The North Pennine batholith (Weardale Granite) of northern England: new data on its age and form. Proc. Yorks. Geol. Soc. 58, 107–128.
Lambert, R.St.J., McKerrow, W.S., 1976. The grampian orogeny. Scott. J. Geol. 12, 271–292.
Law, R.D., Strachan, R., Thirlwall, M., Thigpen, J.R., 2024. The Caledonian Orogeny: late ordovician-early Devonian tectonic and magmatic events associated with closure of the Iapetus Ocean. In: Smith, M., Strachan, R.A. (Eds.), The Geology of Scotland, 5th edition. Geological Society, London, pp. 205–257.
Leake, R.C., Cooper, C., 1983. The Black Stockarton Moor Subvolcanic complex, Galloway. J. Geol. Soc. Lond. 140, 665–676.
Leake, R.C., Brown, M.J., Date, A.R., Smith, T.K., 1977. A Reconnaissance Geochemical Drainage Survey of the Criffel-Dalbeattie Granodiorite Complex and its Environs. Institute of Geological Sciences, p. 116.
Leggett, J.K., 1987. The Southern Uplands as an accretionary prism: the importance of analogues in reconstructing palaeogeography. J. Geol. Soc. Lond. 144, 737–751.
Leggett, J.K., McKerrow, W.S., Casey, D.M., 1982. The anatomy of a lower palaeozoic accretionary forearc: the southern Uplands of Scotland. In: Leggett, J.K. (Ed.), Trench-Forearc Geology: Sedimentation and Tectonics on Modern and Ancient Active Plate Margins, vol. 10. Geological Society, London, pp. 495–520. Special Publications.
MacGregor, M., 1937. The western part of the Criffell–Dalbeattie igneous complex. Q. J. Geol. Soc. 93, 457–486.
Magni, V., Allen, M.B., van Hunen, J., Bouilhol, P., 2017. Continental underplating after slab break-off. Earth Planet. Sci. Lett. 474, 59–67.
McCay, A.T., Younger, P.L., 2017. Ranking the geothermal potential of radiothermal granites in Scotland: are any others as hot as the Cairngorms? Scott. J. Geol. 53, 1–11.
McDonough, W.F, Sun, S.-S., 1995. The composition of the Earth. Chem. Geol. 120, 223–253.
McKerrow, W.S., MacNiocaill, C., Dewey, J.F., 2000. The Caledonian orogeny redefined. J. Geol. Soc. Lond. 157, 1149–1154.
Miles, A.J., Woodcock, N.H., 2018. A combined geochronological approach to investigating long lived granite magmatism, the shap granite, UK. Lithos 304–307, 245–257.
Miles, A.J., Graham, C., Hawkesworth, C., Gillespie, M., Dhuime, B., Hinton, R., 2014. Using zircon isotope compositions to constrain crustal structure and pluton evolution: the iapetus suture zone granites in Northern Britain. J. Petrol. 55, 181–207.
Miles, A.J., Woodcock, N.H., Hawkesworth, C.J., 2016. Tectonic controls on post-subduction granite genesis and emplacement: the late Caledonian Suite of Britain and Ireland. Gondwana Res. 39, 250–260.
Milne, E.J.M., Neill, I., Bird, A.F., Millar, I.L., McDonald, I., Dempsey, E.D., Olive, V., Odling, N., Waters, E.C., 2023. Caledonian hot zone magmatism in the "Newer Granites": insight from the Cluanie and Clunes Plutons, Northern Scottish Highlands. J. Geol. Soc. Lond. 180, jgs2022-076.
Neill, I., Meliksetian, K., Allen, M.B., Navasardyan, G., Kuiper, K., 2015. Petrogenesis of mafic collision zone magmatism: the armenian sector of the Turkish–Iranian Plateau. Chem. Geol. 403, 24–41.
Neilson, J.C., Kokelaar, B.P., Crowley, Q.G., 2009. Timing, relations and cause of Plutonic and Volcanic activity of the Siluro-Devonian post-collision magmatic episode in the Grampian Terrane, Scotland. J. Geol. Soc. Lond. 166, 545–561.
O'Connor, P.J., 1975. Rb-Sr whole-rock isochron for the newry granodiorite, NE Ireland. Sci. Proc. R. Dublin Soc. A5, 407–413.
Oliver, G.J.H., Wilde, S., Wan, Y., 2008. Geochronology and geodynamics of Scottish granitoids from the late neoproterozoic break-up of Rodinia to Palaeozoic collision. J. Geol. Soc. Lond. 165, 661–674.
O'Reilly, B.M., Hauser, F., Readman, P.W., 2012. The fine-scale seismic structure of the upper lithosphere within accreted Caledonian lithosphere: implications for the origins of the 'Newer Granites'. J. Geol. Soc. Lond. 169, 561–573.
Paton, C., Hellstrom, J., Bence, P., Woodhead, J., Hergt, J., 2011. Iolite: freeware for the visualisation and processing of mass spectrometric data. J. Anal. At. Spectrom. 26, 2508.
Pearce, J.A., Bender, J.F., De Long, S.E., Kidd, W.S.F., Low, P.J., Güner, Y., Saroglu, F., Yilmaz, Y., Moorbath, S., Mitchell, J.G., 1990. Genesis of collision volcanism in Eastern Anatolia, Turkey. J. Volcanol. Geotherm. Res. 44, 189–229.
Rapp, R.P., Watson, E.B., 1995. Dehydration melting of metabasalt at 8–32 kbar: implications for continental growth and crust-mantle recycling. J. Petrol. 36, 891–931.
Rapp, R.P., Watson, E.B., Miller, C.F., 1991. Partial melting of amphibolite/eclogite and the origin of Archean trondhjemites and tonalites. Precambrian Res. 51, 1–25.
Rice, S., Cuthbert, S.J., Hursthouse, A., 2018. Tectono-magmatic controls of post-subduction gold mineralisation during late Caledonian soft continental collision in the Southern Uplands-Down-Longford Terrane, Britain, and Ireland: a review. Ore Geol. Rev. 101, 74–104.
Richards, J.P., 2009. Postsubduction porphyry Cu-Au and epithermal Au deposits: products of remelting of subduction-modified lithosphere. Geology 37, 247–250.
Selby, D., Conliffe, J., Crowley, Q.G., Feely, M., 2008. Geochronology (Re-Os and U-Pb) and fluid inclusion studies of molybdenite mineralisation associated with the Shap, Skiddaw and Weardale granites, UK. Appl. Earth Sci. 117. https://doi.org/10.1179/174327508X309669.
Sláma, J., Košler, J., Condon, D.J., Crowley, J.L., Gerdes, A., Hanchar, J.M., Horstwood, M.S.A., et al., 2008. Plešovice zircon — a new natural reference material for U–Pb and Hf isotopic microanalysis. Chem. Geol. 249, 1–35.
Soper, N.J., Strachan, R.A., Holdsworth, R.E., Gayer, R.A., Greiling, R.O., 1992. Sinistral Transpression and the Silurian closure of Iapetus. J. Geol. Soc. Lond. 149, 871–880.
Spencer, C.J., Kirkland, C.L., Taylor, R.J.M., 2016. Strategies towards statistically robust interpretations of in situ U–Pb zircon geochronology. Geosci. Front. 7, 581–589.
Stacey, J.S., Kramers, J.D., 1975. Approximation of terrestrial lead isotope evolution by a two-stage model. Earth Planet. Sci. Lett. 26, 207–221.
Stone, P., 2024. Middle Ordovician-Silurian: Midland Valley forearc basins and the Southern Uplands accretionary complex at the southern margin of Laurentia. In: Smith, M., Strachan, R.A. (Eds.), The Geology of Scotland, 5th edition. Geological Society of London, pp. 171–204.
Stone, P., McMillan, A.A., Floyd, J.D., Barnes, R.P., Phillips, E.R., 2012. British Regional Geology: South of Scotland. Natural Environment Research Council, Keyworth, Nottingham, p. 264.
Strachan, R.A., Alsop, G.O., Ramezani, J., Frazer, R.E., Burns, I.M., Holdsworth, R.E., 2020. Patterns of silurian deformation and magmatism during sinistral oblique convergence, Northern Scottish Caledonides. J. Geol. Soc. Lond. 177, 893–910.
Thirlwall, M.F., 1979. The Petrochemistry of the British Old Red Sandstone Volcanic Province. Unpublished PhD thesis,. University of Edinburgh, p. 477.
Thirlwall, M.F., 1982. Systematic variation in chemistry and Nd-Sr isotopes across a Caledonian calc-alkaline volcanic arc: implications for source materials. Earth Planet. Sci. Lett. 58, 27–50.
Thirlwall, M.F., 1988. Geochronology of late Caledonian magmatism in Northern Britain. J. Geol. Soc. Lond. 145, 951–967.
Tindle, G., McGarvie, D.W., Webb, P.C., 1988. The role of hybridization and crystal fractionation in the evolution of the Cairnsmore of Carsphairn intrusion, Southern Uplands of Scotland. J. Geol. Soc. Lond. 145, 11–21.
Turner, S., Sandiford, M., Foden, J., 1992. Some geodynamic and compositional constraints on "postorogenic" magmatism. Geology 20, 931–934.
Van Hunen, J., Allen, M.B., 2011. Continental collision and slab break-off: a comparison of 3-D numerical models with observations. Earth Planet. Sci. Lett. 302, 27–37.
Villa, I.M., De Bièvre, P., Holden, N.E., Renne, P.R., 2015. IUPAC-IUGS recommendation on the half life of 87Rb. Geochim. Cosmochim. Acta 164, 382–385.

Waldron, J.W.F., Schofield, D.I., Dufrane, S.A., Floyd, J.D., Crowley, Q.G., Simonetti, A., Dokken, R.J., Pothier, H., 2014. Ganderia–Laurentia collision in the Caledonides of Great Britain and Ireland. J. Geol. Soc. Lond. 171, 555–569.

Waldron, J.W.F., Dufrane, A.S., Schofield, D.I., Barr, S.M., White, C.E., 2024. Is Britain divided by an Acadian suture? Geol. Soc. Am. Abstr. Programs 56. https://doi.org/10.1130/abs/2024NE—397307.

Watson, E.B., Wark, D.A., Thomas, J.B., 2006. Crystallization thermometers for zircon and rutile. Contrib. Mineral. Petrol. 151, 413–433.

Wiedenbeck, M., Allé, P., Corfu, F., Griffin, W.L., Meier, M., Oberli, F., Von Quadt, A., Roddick, J.C., Spiegel, W., 1995. Three natural zircon standards for U-Th-Pb, Lu-Hf, trace element and ree analyses. Geostand. Newslett. 19, 1–23.

Williams, H.M., Turner, S.P., Pearce, J.A., Kelley, S.P., Harris, N.B.W., 2004. Nature of the source regions for post-collisional, potassic magmatism in Southern and Northern Tibet from geochemical variations and inverse trace element modelling. J. Petrol. 45, 555–607.

Wolf, M.B., Wyllie, P.J., 1994. Dehydration-melting of amphibolite at 10 kbar: the effects of temperature and time. Contrib. Mineral. Petrol. 115, 369–383.

Woodcock, N.H., Soper, N.J., Strachan, R.A., 2007. A Rheic cause for the Acadian deformation in Europe. J. Geol. Soc. Lond. 164, 1023–1036.

Woodcock, N.H., Soper, N.J., Miles, A.J., 2019. Age of the Acadian deformation and Devonian granites in Northern England: a review. Proc. Yorks. Geol. Soc. 62, 238–253.